The Hong Kong Polytechnic University

Department of Civil and Structural Engineering

APPLIED PHOTOGRAMMETRY FOR 3D MODELING, QUANTITY SURVEYING, AND AUGMENTED REALITY IN CONSTRUCTION

By

FEI DAI

A Thesis Submitted in Partial Fulfilment of the Requirements for the Degree of Doctor of Philosophy

October 2009

CERTIFICATE OF ORIGINALITY

I hereby declare that this thesis is my own work and that, to the best of my knowledge and belief, it reproduces no material previously published or written, nor material that has been accepted for the award of any other degree or diploma, except for where due acknowledge has been made in the text.

_________________________________(Signed)

_____________Fei Dai_____________(Name of student) *for my parents*

ABSTRACT

The surveying technique of close-range photogrammetry is based on an analytical representation of the image forming mechanism of photography and extracts spatial information through computation on photos. This research reviews the fundamentals of close-range photogrammetry and applies close-range photogrammetry to (1) model 3D construction graphics, (2) measure the geometric dimensions of building products, and (3) augment site photos with 3D graphics of underground facilities.

This research firstly establishes a 3D modeling method based on the mechanism of photogrammetry to ease the effort in providing model ingredients for visualizing main processes and major products in construction operations. The current way of 3D modeling, which relies on the use of computer-aided design (CAD) or proprietary software for virtual reality (VR) development, not only requires object design drafts or geometry specifications to be prepared beforehand, but also has a tedious, time-consuming procedure. The proposed method utilizes a digital camera to capture site images and analytically processes the image data into a 3D model of an object, by which the effort of modeling is largely alleviated. A precast façade is modeled under practical constraints to verify the method. The method is useful particularly when the design drafts or geometry specifications of the modeling

objects are unavailable or the modeling objects are inaccessible for direct measurement due to safety concerns.

The photo-based 3D as-built modeling method provides an alternative to taking geometric measurements on building products. In contrast with the conventional measurement tape, applying photogrammetry is cost-effective and safe as the measurements are conducted on the 3D model of an object resulting from photos, instead of on the object itself. Thus, the proposed method is conducive to measuring the building elements situated in hazardous areas and quickly checking the dimensions of precast units on site for quality control purposes. The measurement errors of the photo-based method are attributed to (1) the systematic error due to camera lens distortions and (2) the random error due to human factors. Seventy-nine paired measurements (length, width, and height) are sampled on twelve structures and facilities by applying the photo-based method and measurement tape respectively. The 95% limits of agreement are established on the sample data to statistically characterize the accuracy level of the photo-based method against tape, resulting in [-15.30 mm, 11.39 mm]. Through weighing the accuracy level against the accuracy level desirable in a particular application, the engineer makes the final decision on the applicability of the photo-based method.

In addition, this research adapts the analytical algorithms of photogrammetry into a computationally simple yet practical method for incorporating computer-generated, three-dimensional (3D) as-built graphics of invisible underground infrastructure into site photos, resulting in a richer and more integral view of the site situation. Previous photo-augmenting methods require both the camera's position and orientation to be determined on site. The new method simplifies the superimposition of a view taken from a 3D virtual model onto an actual photo by analytically fixing the camera's orientation with the coordinates of two reference points only, namely, the camera station position and the object focus position. The advantage of the proposed method over current photo-augmenting techniques lies largely in alleviating the effort required for camera positioning in the field. By setting a virtual camera in the 3D modeling environment in the same way as the site photo is actually taken, a virtual view of the underground scene is produced, which is then analytically merged with the site photo by coinciding the real and virtual coordinate axes in the two-dimensional (2D) image space. The new approach has been applied to superimpose as-built models of infrastructure onto site photos in order to facilitate quality check of bored pile excavation and progress visualization of micro-tunneling construction. The level of accuracy for augmented photo registration depends on the specific implementation settings on site including the surveying instrument applied and the camera used. As for the bored pile excavation and micro-tunneling cases conducted in this research, given the exact coordinates of the camera station position and the object focus position, the augmented photo registration can achieve an accuracy level of 0.07 mm on the camera image plane.

PUBLICATIONS

PEER REVIEWED JOURNAL ARTICLES

1. **Dai, F.**, and Lu, M. (2010). “3D modeling of site elements by analytically processing image data contained in site photos.” *Journal of Construction Engineering and Management*. Reston, VA: ASCE. (in review)

2. **Dai, F.**, Lu, M., and Kamat, V. R. (2010). “Analytical approach to augmenting site photos with 3D graphics of underground infrastructure in construction engineering applications.” *Journal of Computing in Civil Engineering*. Reston, VA: ASCE. (in press)

3. **Dai, F.**, and Lu, M. (2010). “Assessing the accuracy of applying photogrammetry to take geometric measurements on building products.” *Journal of Construction Engineering and Management*, 136(2), 242-250. Reston, VA: ASCE.

PEER REVIEWED CONFERENCE PAPERS

4. **Dai, F.**, and Lu, M. (2009). "Analytical approach to augmenting site photos with 3D as-built bored pile models." In *Proceedings of the 2009 Winter Simulation Conference*, eds. M. D. Rossetti, R. R. Hill, B. Johansson, A. Dunkin, and R. G. Ingalls, 2691-2702. Austin, Texas, USA: IEEE.

5. **Dai, F.**, and Lu, M. (2008). "Photo-based 3D modeling of construction resources for visualization of operations simulation: case of modeling a precast façade." In *Proceedings of the 2008 Winter Simulation Conference*, ed. S. J. Mason, R. Hill, L. Moench, and O. Rose, 2439-2446. Miami, Florida, USA: IEEE.

6. **Dai, F.**, and Lu, M. (2008). "Photogrammetry-based three-dimensional modeling of construction resources: error definition and measurement." *12th International Conference on Computing in Civil and Building Engineering & 2008 International Conference on Information Technology in Construction (ICCCBE-XII & INCITE 2008)*, October 16-18, 2008. Beijing, China.

ACKNOWLEDGEMENTS

I am thankful to my chief advisor, Professor Ming Lu for his supervision, inspiration, wisdom, and friendship. Over the past four years and ten months, he has advised me with numerous ideas, suggestions and criticisms as well as his profound knowledge in the field of construction engineering and management. I am also grateful to my co-advisor, Professor Wu Chen, who has provided me with valuable suggestions and constructive comments during my study of photogrammetry.

I would like to express my gratitude to the Research Grants Committee (RGC) of Hong Kong for partially funding the research under Project PolyU 5245/08E, and the Department of Civil and Structural Engineering at the Hong Kong Polytechnic University for providing academic resources to this research.

I am grateful to Tom Hung and Stephen Cheng who work with Ove Arup Hong Kong Ltd. for sharing their insight and experience and assisting me in conducting research-verification experiments in practical construction sites.

Special thanks to Professor Vineet R. Kamat, who received me as a visiting scholar at the University of Michigan during my study period. This not only broadens my view on the cutting-edge IT technology applied in construction but also increases my interest and confidence in this research area.

Thanks also to all members of the construction research group under Professor Lu at the Hong Kong Polytechnic University. Ideas were shared and exchanged by numerous group meetings and discussions. They are: Xuesong Shen, Xiong Liang, Hoi-Ching Lam, Ming-Fung Siu, Sze-Chun Lau, and Wah-Ho Chan.

Most of all, thanks to my parents and my girlfriend for their enormous support, encouragement, and understanding. Without them, this research work could not have been accomplished.

TABLE OF CONTENTS

LIST OF FIGURES

LIST OF TABLES

CHAPTER 1

INTRODUCTION

1.1 INTRODUCTION

Chapter 1 provides an overview of the thesis, including research background, objectives, scope, and outline of the dissertation. This chapter first introduces the current state in construction research and briefs on the research incentives. Then the major goals to be achieved in this research are outlined, and the research scope is defined. Last, this chapter provides a snapshot of each of the six chapters in the dissertation.

1.2 RESEARCH BACKGROUND

It is widely recognized that the construction industry is challenging and competitive (Halpin and Riggs 1992; Hampson and Tatum 1997; Gould and Joyce 2002). Over the past decades, construction has evolved with numerous innovations in order to seek for improvement. A plethora of cutting-edge technologies have been customized and applied in practice and research. Examples include Discrete-Event Simulation

(DES) (Halpin 1977; Martinez and Ioannou 1999; Lu 2003), 4D Computer-Aided Design (4D-CAD) (McKinney et al. 1996; Koo and Fischer 2000; Zhang et al. 2000; Akinci et al. 2002), dynamic and animated 3D visualization (Kamat and Martinez 2001), Augmented Reality (AR) (Dunston and Wang 2005), 4D Augmented Reality (4D-AR) (Golparvar-Fard and Peña-Mora 2007; Lee and Peña-Mora 2006), automatic and autonomous monitoring of building structures (Moore 1992), image reasoning (Brilakis and Soibelman 2005), Dynamic Data Driven Application Systems (DDDAS) (Lu et al. 2007), to name but a few. Nonetheless, the surveying technique of photogrammetry has only sporadically fallen on the screen of construction researchers' radar, with a few applications found in the literature.

To account for this situation, the possible reasons are identified: (1) sophisticated analytics underlying this technology hinder the use by the construction professionals, most of whom are not well conversant with complicated mathematical equations of surveying; (2) lack of application guidance of the well-established photogrammetric theory to the construction discipline; and (3) research on applied photogrammetry has yet to mature for the widespread use of this technique in construction industry.

On construction sites, changes constantly take place with the evolution of a construction project. The digital photos have been largely used to keep timely records of construction progress and provide evidence of site problems. With site photos, a particular state of the site situation, including building products, construction resources and the site layout, can be easily captured. Meanwhile, recent advances in electro-optical technologies have empowered the off-the-shelf digital cameras to obtain high quality images, while maintaining portability and convenience of taking pictures. The price tag of digital cameras has been removed and the digital photography technique can be deemed as a convenient way for site data collection without interfering with the ongoing construction operations nor imposing extra workload that needs to be performed before, during, or after the use of this technology (Akinci et al. 2006; Golparvar-Fard et al. 2009).

Current applications of digital photos in construction site management mainly fall in the 2D scope. The site engineers are also in need of using the 2D images to extract 3D information like the position of the site element and the dimension of the building product. The surveying technique of photogrammetry is well established to fulfill such need. Processing 2D photos, photogrammetry is capable of taking non-contact measurements of objects and establishing spatial relationships between the objects in the three-dimensional (3D) space. By using a digital camera, photogrammetry allows site engineers to easily acquire photos on site and interpret image data in office. This technique retains instrumental portability for as-built data collection while significantly reducing the manpower resources required in the field. With the 3D points fixed by the photo-based 3D re-construction, spatial information of building products and site elements can be easily calculated based on the coordinates of a limited quantity of known points.

Photogrammetry holds great potential to serve as a supplementary or supportive means for addressing conventional problems of site administration and improving engineering performances in construction, such as quantity surveying on as-built building products, dimension checking on prefabricated building elements for quality control, and visualization of project progress and site operations. However, the photogrammetry technique is only mastered by the surveying professionals who may lack the knowledge and experience in construction engineering and management. On the other hand, the analytical complexity underlying photogrammetry presents obstacles that have kept construction professionals from employing this technique. This research makes an attempt to bridge the two areas and promote photogrammetry for the use in construction applications.

1.3 RESEARCH OBJECTIVES

This research is intended to utilize the analytical power of the surveying technique of photogrammetry to address practical construction problems and improve the practice of construction management. The detailed objectives are stated as follows:

- Establishing a photo-based 3D as-built modeling method using the analytics of photogrammetry to save the time and effort in providing the model ingredients for dynamic 3D visualization of construction operations; also providing an analytical foundation for further utilization of photogrammetry in quantity surveying and augmented reality in construction applications.

- Quantitatively assessing the accuracy of the photo-based 3D modeling method in checking the dimensions on prefabricated building units for quality control and taking geometric measurements on building products and site elements situated in hazardous areas that are unsafe to access.

- Adapting the photogrammetric mathematics to the application of augmenting the site photos with 3D graphics of underground infrastructure, so as to provide richer and more integral views that include both ground and underground information for better investigation of foundation excavation and visualization of project progress.

1.4 RESEARCH SCOPE

According to camera position and object distance, photogrammetry can be grouped into five categories - satellite, aerial, terrestrial, close-range, and macro (Luhmann et al. 2006). The study of this research falls into the category of close-range photogrammetry, which usually applies to those situations where the target object is away from the camera at a distance ranging from 1 m to 300 m (Luhmann et al. 2006).

This research discusses the digital photogrammetry. This means this research employs modern digital cameras to capture image data instead of old, conventional film cameras. Also, the quality of the camera used affects the goodness of the measurement results achieved. This research does not consider the use of high-end, expensive cameras but employs the off-the-shelf, portable digital cameras, with which construction professionals can take snapshots conveniently on site.

1.5 DISSERTATION OUTLINE

Chapter 2 reviews the photogrammetry fundamentals and analyzes the advantages of applying photogrammetry for construction practices, based on which the research gaps are identified and the research methodology is proposed.

Chapter 3 studies the photogrammetry analytics, based on which, a photo-based 3D modeling method is developed, capable of analytically processing the image data contained in site photos of a site element into a 3D model.

Chapter 4 analyzes the major factors that affect the photogrammetric measurement results and assesses the accuracy of applying photogrammetry to take geometric measurements on building products.

Chapter 5 adapts the photogrammetric analytics and proposes a practical method to augment site photos with 3D graphics of underground infrastructure in construction engineering applications.

Chapter 6 summarizes the research in terms of contributions and limitations, and recommends future extensions.

1.6 SUMMARY

This chapter briefly describes the research, including the research background, research objectives, and research scope, and the organization of the dissertation. A review of photogrammetry along with the research methodology is presented in the next chapter.

CHAPTER 2

LITERATURE REVIEW

2.1 INTRODUCTION

Chapter 2 addresses the question why this research is conducted, in which the photogrammetry fundamentals and applications are reviewed, and the research gaps of applying photogrammetry in construction practices are identified. Finally, this chapter proposes the research methodology.

2.2 PHOTOGRAMMETRY FUNDAMENTALS

2.2.1 Definition

Aimé Laussedat who is referred as the "father of photogrammetry" laid the foundation of photogrammetry in the middle 1800s and Albrecht Meydenbauer coined the term "photogrammetry" in the late 1800s (Blachut and Burkhardt 1989). Generally, photogrammetry is the discipline of performing indirect measurements of natural space by using photography, and entails the process of extracting data from

2D images and mapping them onto the 3D space (Blachut and Burkhardt 1989).

The digital photogrammetry can be referred to as the way that the photographs or videos, which are captured by digital cameras or camcorders and stored in storage media, are accessed in computer workstations and processed by photogrammetric software to determine the spatial relationships or obtain the measurements of objects. The digital photogrammetry largely facilitates the use of this technology in a wide range of scientific and engineering applications.

2.2.2 Categorization of Photogrammetry

Photogrammetry can be categorized in a multitude of ways. Table 2-1lists a general categorization of photogrammetry.

Table 2-1 Categorization of photogrammetry (Luhmann et al. 2006)

By camera position and object distance	
- Satellite photogrammetry	Processing of satellite images, h > *ca.* 200 km
- Aerial photogrammetry	Processing of aerial photographs, h > *ca.* 300 m
- Terrestrial photogrammetry	Measurements from a fixed terrestrial location
- Close range photogrammetry	Imaging distance h < *ca.* 300 m
- Macro photogrammetry	Microscope imaging, image scale > 1
By number of measurement images	
- Single image photogrammetry	Single image processing
- Stereo photogrammetry	Dual image processing
- Multi-image photogrammetry	N images where N > 2
By method of recording and processing	
- Plane table photogrammetry	Graphical evaluation (until *ca.* 1930)
- Analogue photogrammetry	Analogue cameras, opto-mechanical measurement systems (until *ca.* 1980)
- Analytical photogrammetry	Analogue images, computer-controlled measurement
- Digital photogrammetry	Digital images, computer-controlled measurement
- Videogrammetry	Digital image acquisition and measurement
- Panorama photogrammetry	Panoramic imaging and processing
- Line photogrammetry	Analytical methods based on straight lines and polynomials
By availability of measurement results	
- Real-time photogrammetry	Recording and measurement completed within a specified time period particular to the application
- Off-line photogrammetry	Sequential, digital image recording, separated in time or location from measurement
- On-line photogrammetry	Simultaneous, multiple, digital image recording, immediate measurement

Note: *ca.* is a Latin abbreviation for “approximately”.

2.2.3 Mechanism

The mechanism of photogrammetry explains the process of transforming images into spatial 3D information. Fig. 2-1 illustrates the sequences of the process in which data (images) are acquired, measured, and interpreted. The left hand side indicates the instrumentation used in the process and the right hand side implies human knowledge, experience, and skills as required.

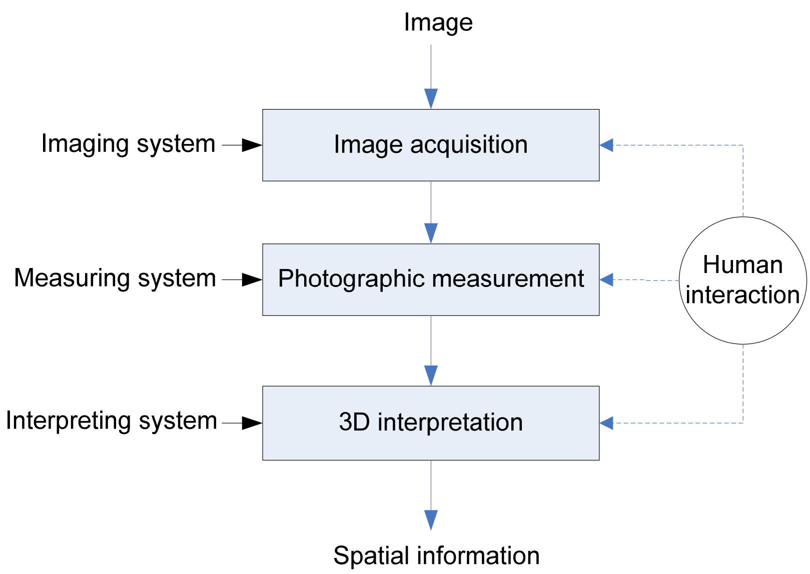

Fig. 2-1 Photogrammetric process from image to spatial information

The image acquisition describes the image forming process by which an image is created. The imaging system can be referred to as a collection of digital cameras and computer memories that store the image data. The image forming process concerns the interior orientation (describing the internal geometric parameters of a camera) and the exterior orientation (specifying the spatial position and orientation of the camera). Two orientations determine the parameters of the camera necessary to transform the spatial point in the global space into the image point on the image plane. As rays of light pass through the lens opening of a camera, an image framing a scene of interest is produced and stored in the computer memory ready for computer processing.

Prior to analyzing the spatial information, photographic measurements on the images need to be performed to identify the input for photogrammetric equations. The photographic measurements include the lengths of lines between points, angles between points, or positions of points on images expressed in the form of rectangular coordinates. Rectangular coordinates are the most common type used for photographic measurements and can be directly applied in photogrammetric equations. A variety of simple and advanced instruments are available for the photographic measurement, e.g., microruler, monocomparator (Wolf 1983). In the era of digitization, the coordinates of image points can be measured through the pixels and computer vision techniques; for example, Scale Invariant Feature Transforms (SIFT) algorithm (Lowe 2004) can be used to accomplish the identification of the desired image points.

In forming a photo image, the transformation of a higher-dimensional (3D) space to the lower-dimensional (2D) image give rise to a loss of information. Any point on the image and its corresponding spatial point in the global space can be linked by a ray of light. However, the length of the ray between the two points is initially unknown, i.e. all spatial points lying on the ray of light are projected as the same point in the image. The 3D interpretation is to determine the 3D coordinates of the spatial point that correlates the image point using photogrammetric equations. The spatial point is located on the ray of light and determined in the global space by intersecting the ray with additional known geometric elements such as a second ray of light or an object plane. Further manipulating the spatial points obtained yields the spatial information desired (e.g., line, triangular, rectangle) or dimensions (e.g., distance, area).

2.2.4 Tools

Easy-to-use software tools facilitate object reconstruction and creation of virtual 3D models from digital images without requiring the domain knowledge of photogrammetry. This lends itself well for both practitioners and researchers to adopt photogrammetry to solve practical problems. Currently, there is well-established software prevailing both in industrial markets and in research fields. As for close-range photogrammetry software systems, there are PhotoModeler® (Eos Systems Inc. 2007), ImageModeler® (REALVIZ S.A. 2007), and iWitness® (PhotoMetrix 2007). These software packages provide the functionality of performing photographic measurements on photo pixels and calculating 3D dot arrays for image points for ease of applications in a wide range of industry sectors and research areas, including architecture preservation, archaeological exploration, medical inspection, accident reconstruction, animation, forensics, and plant and mechanical engineering. This research employs PhotoModeler® as the photogrammetric tool in developing photo-based 3D modeling methodologies and verifying solutions tailor-made for specific construction problems.

2.3 PHOTOGRAMMETRY APPLICATIONS

2.3.1 Status of Photogrammetry Applications

Close-range photogrammetry has been applied in several scientific and engineering applications. These applications can be categorized as:

- Architecture and heritage preservation.

  Advances in architectural modeling was made by Almagro et al. (1996) on modeling the Otto Wagner Pavilion in Vienna which is used by CIPA (one of the oldest International Scientific Committees of ICOMOS - the International Council on Monuments and Sites) as a reference building for testing modern methods of measurement and processing in architectural photogrammetry. By applying close-range photogrammetry techniques, Arias at el. (2006) combined the graphic and metric documentation on the traditional agro-industrial buildings which are an important part of the heritage of Galica (northwest of Spain).

- Forensics and accident reconstruction

  Fenton and Ziernicki (1999) determined a vehicle crash and equivalent barrier speed by creating three-dimensional computer models of damaged vehicles utilizing photographs. Based on general bodily features, gait and anthropometric measurements, Lynnerup and Vedel (2005) managed to use photogrammetry to help the police correctly identify the perpetrator of a bank robbery by performing measurements of height, angle for gait analysis.

- Industrial applications

  Przybilla et al. (1988, 1990) used photogrammetry to determine the shapes of a fuel assembly, which was an essential part of a nuclear power plant and could only be handled underwater. Besides, the determination of deformation of industrial tooling (Beyer et al. 1995, Fraser 1996) and deformation monitoring of a series of super-hot steel beams (Fraser and Riedel 2000) by digital close-range photogrammetry were reported. In addition, examples also include automatic shape measurement and accuracy control in areas of car industry (e.g., Riechmann and Ringel 1995) and ship industry (e.g., Schneider 1994).

- Medical applications

  Photogrammetric measurement has been used on the face more than on any other part of the body (Mitchella and Newton 2002). For instance, it was made to monitor facial shape as it changed over an extended period of time through growth (e.g., Burke and Beard 1979). Before and after surgery, photogrammetry was used in investigating changes over this short period of time (Coombes et al. 1990). Furthermore, photogrammetry was involved in the therapy of various gait problems arising primarily from deformities or injuries (Walton 1990) and sport movement in respect of golf, tennis, and football (e.g., Chikatsu et al. 1992).

- Engineering applications

  With respect to engineering applications, photogrammetry has been largely applied in the areas of deformation monitoring and profile measurement. Deformation monitoring is usually used to measure deformations on structures or facilities that are exposed to particular mechanical or thermal strain.

Examples include use of photogrammetry for more accurate measurement in pavement deformation monitoring (Mills et al. 2001), and automated image processing techniques to help understand the evolution of cracks in concrete structures under long term natural deformation (Dare et al. 2002). Profile measurement in engineering primarily involves measurement of structure interiors or surfaces for shape analysis and documentations. One such example is the experimental photogrammetric wriggle surveying in the Second Mersey Tunnel in 1970 (Proctor and Atkinson 1972).

2.3.2 Benefits of Applying Photogrammetry

From the above photogrammetric applications, the benefits of applying photogrammetry are identified as follows:

- Input data are recorded in photographs. In contrast to “as-designed” data like CAD drawings, the “as-built” photographs realistically capture and keep the status of a jobsite pertaining to building products, construction resources, and site layout at a certain point of time, which can be used as valuable information for further site investigation and progress monitoring.

- Spatial (3D coordinates) and geometric (length, width, height) measurements can be accomplished without touching the measured object itself. The measurements are conducted directly on photos. This enables (1) taking measurements on those building elements situated in hazardous areas that are unsafe to access and (2) continuously monitoring the alignments of a building product by taking site pictures at different times.

- Cost-effective and convenient setup of instrument makes this technique easy-to-apply. Only affordable, off-the-shelf digital cameras are required to collect the data, which does not interfere with the ongoing construction operations in field.

For these reasons, photogrammetry has been explored and applied in several construction engineering applications, which will be discussed in the next section.

2.3.3 Related Work in Construction Engineering Applications

To ameliorate managerial and operational capabilities, digital photos have been long applied in the process of the conventional construction production. Examples include (1) generation of a panorama view of the site situation by seamlessly linking a series of site pictures (Waugh 2006), (2) development of a construction control system by integrating the site construction progress bar chart in MS Project with a database of site pictures showing the building process and building elements at particular points of time (Abeid et al. 2003), and (3) advancement of a time-lapse photography technique for project management by recording activities in a construction site with a series of photographs, enabling playback at optional frame rates (Abeid and Arditi 2002a, 2002b). These applications proved the effectiveness of using the imagery technology for recoding, keeping, and analyzing the varying and dynamic site situations during construction.

Preliminary efforts have been made to apply photogrammetry to construction for quantity takeoff and progress control. Kim and Kano (2008) developed photo images in 3D computer graphics showing the "as-built" site situation at a particular time.

Those photo-based models were compared against the corresponding as-planned CAD images, which were captured from the construction plan visualized in a virtual reality system. The research used fixed-position cameras to take the site photos, in which more than one camera were involved for the instrumental setup and additional surveying apparatus were used to fix the positions of cameras and marking points on the building product. Application cases in foundation excavation, refill, scaffolding and steel erection proved their methodologies to be convenient and effective in checking actual site progress against as-designed or as-planned models. Memon et al. (2005) prototyped a digitized construction monitoring system, aimed at monitoring and evaluating actual construction progress. Progress percentage was calculated by comparing a 3D building object extracted from site photos against its design drawings in AutoCAD. Quiñones-Rozo et al. (2008) used digital photogrammetry to retrieve the 3D model for an excavation site and track activity progress on a residential project. Zhu and Brilakis (2009) reconstructed a house and a wheel loader as two example cases validating photogrammetry as an optical sensor-based spatial data collection technique for civil infrastructure modeling. These applications reflect the increasing importance of using photo contents to keep current status of the site and help site engineers control changes and progress in construction.

Researchers have also explored the application of imaging techniques to acquire geometric information from photos for measuring the differences on building products between two temporal states. Site photos were analytically processed by contractors to measure 3D geometries of buildings adjacent to a construction site (Luhmann and Tecklenburg 2001). The intention was to preserve forensic evidence against potential construction-caused damage claims. Kamat and El-Tawil (2007) performed lab experiments on measuring and interpreting the drifts between the original walls in 3D CAD images and the actual wall specimens for post assessing any earthquake-induced building damages. Mok et al. (1998) investigated the application of photogrammetric techniques combined with GPS georeferences, leading to development of image processing algorithms for large scale site mapping from digital imagery. These research endeavors are all concerned with mapping spatial data from a two-dimensional photo image onto a three-dimensional virtual space and quantifying geometric offsets based on the photo-derived models.

2.3.4 Research Gaps

Previous construction applications have mainly focused on attaining desired accuracy in measurements so as to support quantity take-off and determine progress percentage in construction project management. In general, conducting site-based case studies entails fixing a high-end, specially calibrated digital camera on a tripod, which is placed at a proper spot in the site. The coordinates of each tripod spot and each control point need to be precisely determined in order to calibrate the camera parameters needed for space transformation by photogrammetry.

However, the following issues have yet to be clarified with regard to photography and photogrammetry applications in construction:

- A low-cost, point-and-shoot, more flexible photogrammetry technique is yet to be formalized in order to support dynamic visualization of a construction operations plan in the form of a CPM schedule or a process simulation. Models illustrated in previous research were only simple cases (such as box mini-foundation), failing to demonstrate the modeling capability with respect to handling more complex construction products or resources. Mathematical foundations behind applying photogrammetry, along with structured application procedures for modeling complex construction resources, have yet to be clarified.

- The results from quantity take-off by photogrammetry inevitably feature geometric errors. The accuracy of photogrammetry is dependent on the imaging precision of the camera used, the quality of the photos taken, and the functionality of photo-processing algorithms applied. Although photogrammetry holds great potential to provide an alternative to quantity surveying in construction management, a reliable statistical method for assessing the accuracy of geometric measurements taken by photogrammetry is yet to be developed.

- Post-processing image data extracts geometric information from 2D images and establishes spatial relationships between 2D images and the 3D space. This technique can be adapted to various scientific, industrial, engineering practices. As for the adaptation in the area of construction engineering, two aspects are to be addressed, namely: (1) the underlying analytics of the image forming mechanism in photographing has not been enlightened to construction professionals, and (2) the reversed process of immersing 3D as-built models into a photo by computation has yet to be attempted in construction research.

This research makes attempts at filling these research gaps in three parts of studies.

The next section will discuss the three parts of studies, which constitute the research methodology.

2.4 RESEARCH METHODOLOGY

Study 1: To establish a "point-and-shoot" procedure for applying photogrammetry to model the building products and elements on site, minimizing the need for setting up the tripod and measuring the absolute position of the camera and control points.

Transformation from the 2D image data to the 3D object model will be studied by analytically intersecting bundles of rays projected from different camera perspectives in the object space. The camera station's spatial position and orientation, which are prerequisite to the calculation of the bundle intersection, will be determined by cross referencing a limited quantity of feature points marked on different photos.

Experiments will be conducted in which products and elements are modeled at real building sites in 3D by computing on a collection of site pictures so as to evaluate the applicability of photogrammetry for modeling building components as ingredients to generate virtual scenes of construction operations in particular time events. Notably, applications related to modeling complex construction site elements have not yet been particularly addressed in any showcase projects.

In this research, a guide will be developed on (1) how to identify and select reference points on the target object or in its surroundings and (2) how to frame multiple pictures of the target object from different angles, so as to provide input to photogrammetry modeling. The 3D objects to be extracted from site photos will be building elements (such as precast facades).

Study 2: To formalize a statistically significant, quantitatively reliable technique to assess the accuracy of applying photogrammetry in determining configurations and dimensions of a building component.

This entails relating the "lens distortion error" of the camera itself and the "manipulation error" in marking reference points to the limit of error in quantity surveying, and making it comprehendible to construction professionals. The research will produce a guide on how to prepare digital cameras and shed light on whether the choice of a commonly available camera is suitable to enable 3D building component modeling and attain the desired accuracy.

As a result, a site engineer simply takes snapshots of a building product with a digital camera from different angles. Back in office, the engineer derives as-built measurements through post-processing those photos using photogrammetry software. With guidance on working procedures and measurement errors, construction managers will be able to turn site pictures into 3D "as built" models for the fast-changing site situation during the dynamic construction process. Quantity surveying is done simply by defining reference points and reference lengths in digital photos. The availability of such "as-built" photo models could complement the use of quantity takeoff forms and as-built drawings in the current practice.

Subjects related to a building site will be sampled in the modeling experiments, yielding sufficient paired geometric measurements (length, width, and height) by photogrammetry and by measurement tape respectively for the assessment of the accuracy of this surveying method. The biases and limitations of analyzing the agreement between two sets of measurements by regression and correlation coefficient techniques will be first revealed. Then, the "95% limits of agreement" method will be applied on the sample data and the confidence intervals will be established for the limits of agreement derived, so as to ensure validity and statistical significance of the results. In short, the main contribution of this research lies in formalizing a statistically significant, quantitatively reliable technique to assess the accuracy of applying photogrammetry in particular applications of construction engineering. Through weighing the accuracy level achievable by photogrammetry against the accuracy level desirable in a particular application, the engineer makes the final decision on the applicability of the photogrammetry-based approach.

Study 3: To develop an analytical, straightforward, easy-to-apply method to augment site photos with computer-generated 3D graphics which represent the as-built underground infrastructure, so as to present an enriched complete view of the construction site situation in construction engineering applications.

Current practice uses site photos only to capture visible ground information while data of "invisible" underground facilities are mainly archived in paper-based forms or charts. This tends to result in inefficient and inconsistent communications between different parties in addressing problems associated with the built infrastructure.

In an attempt to improve the current construction practice, this research is to propose an analytical approach to augment site photos with computer-generated 3D graphics of the as-built underground infrastructure. Based on computation on the positions of reference points in the coordinate systems of the virtual site and actual site, the presented approach analytically controls a “virtual camera” to take a photo of the 3D as-built model and maps the resulting virtual view onto the site photo, which is a 2D view of actual site. Two case studies are conducted: (1) the underground as-built data is applied to augment a photo of the aboveground site for the purpose of facilitating quality investigation of bored pile construction; in the case of bored pile excavation, the subsurface ultrasonic imaging technologies will be employed for outlining the profile of the underground infrastructure and modeling the 3D as-built models. (2) micro-tunneling site photos are augmented with as-built 3D-CAD models of concrete sleeve pipe to visualize the dynamic progress on the site.

2.5 SUMMARY

This chapter has studied the fundamentals of photogrammetry. Then the applications of photogrammetry in diversified scientific, industrial, and engineering disciplines are introduced. The benefits of applying photogrammetry are also discussed, with particular emphasis on applications in construction. Gaps to be filled through the research are identified. Last, this chapter introduces the research methodology and provides an overview of the entire research.

CHAPTER 3

MODELING THREE-DIMENSIONAL AS-BUILT SITE ELEMENTS BY POINT-AND-SHOOT PHOTOGRAPHY

3.1 INTRODUCTION

This chapter establishes a 3D modeling method based on the mechanism of photogrammetry, which analytically processes the image data contained in site photos into a 3D model for a site element. In contrast with conventional computer-aided design (CAD) or virtual reality (VR) modeling, the proposed method takes advantage of the site photos easily acquired with a digital camera to build 3D models. A minimum of five pairs of image points of the object from two photos taken at two different camera stations provide sufficient input data to analytically derive the positions and orientations of the camera stations. With more than five paired image points available, the least squares adjustment is utilized to refine the modeling results. The mathematical formulas are established for the proposed method, with the computational procedure illustrated with a simple “box” example. To demonstrate the feasibility of the proposed method in practical settings, a case study of modeling a precast façade on a building site is given. In conclusion, the proposed analytical approach for 3D modeling of site elements based on site photos is computationally simple and cost effective to facilitate construction management functions, such as providing the model ingredients for dynamic 3D construction operations visualization, determining the quantities from the as-built models, and checking the dimensions on prefabricated building elements for quality control.

3.2 MODELING 3D SITE ELEMENTS: OVERVIEW

Modeling the three-dimensional (3D) graphics of site elements including building products, equipment, and temporary facilities is indispensible to enabling visualization of main processes and major products in construction operations (Kamat and Martinez 2001). Typically, construction researchers resort to computer-aided design (CAD) or proprietary code for virtual reality (VR) development in order to produce the 3D graphical models for construction resources and facilities (Retik and Shapira 1999; Koo and Fischer 2000; Kamat and Martinez 2001; Al-Hussein et al. 2006). The modeling of complicated site elements in 3D from scratch usually entails a tedious, time consuming procedure, demanding the modeler to define every geometric feature of the model. On the other hand, attaining high precision in 3D modeling, for most cases, is not a crucial issue for construction operations visualization.

At a construction site, practitioners routinely rely on taking site photos to chronicle the evolution of the site and provide evidence to potential problems. The ubiquity of portable digital cameras has made it even more straightforward to record a particular state of the site situation, including building products, construction resources and site layout, without interfering with the site nor imposing much extra workload before, during or after the work (Akinci et al. 2006; Golparvar-Fard et al. 2009).

Based on the image formation mechanism of photography, the surveying technique of photogrammetry analytically acquires geometric information by taking measurements directly on photos (Blachut and Burkhardt 1989). The underlying mathematical equations relate the image coordinate system inside the camera with the object coordinate system in the global space. The very basic technique of this method is effective and computationally simple. With much less effort, digital cameras and photogrammetry software have made possible 3D reconstruction of an object in digital form (coordinates and derived geometric elements). The resultant 3D models may well satisfy application needs in construction.

To implement photo-based 3D modeling of site elements, surveying instruments (such as total station, compass, and gyroscope) are usually required to determine the position and orientation of the camera station where a photo is taken. However, a dynamic, congested construction site, which is always ridden with obstacles such as temporary facilities, partially completed structures, all kinds of resources (equipment, materials and workforce), makes it expensive and difficult to conduct the surveying operations as needed, thus potentially compromising the convenience and cost effectiveness of such applications.

To facilitate photo-based 3D modeling in construction, this research investigates the analytical method for fixing the camera position and orientation by directly computing on photo images acquired. The proposed modeling procedure is as follows: Simply holding a digital camera, an engineer can easily take two snapshots of an object from two angles in the field, with no need to set out the tripod for the camera or any other surveying instruments on site. Then, back in office, the engineer can readily generate a 3D model of the site element by interpreting the photos and analyzes data with the assistance of photogrammetry software. Feature points on the object are marked on the two pictures with x, y coordinates determined in respective picture frames, providing the input to calculate the status parameters of the two camera stations, namely, the three spatial coordinates and the three orientation angles of the camera stations. As such, any point on the object can be mathematically transformed into (X, Y, Z) coordinates in the object space based on its (x, y) coordinates in the picture frames.

The remainder of this chapter presents the analytical algorithms in detail, with the computational procedure illustrated with modeling a “box” in 3D from two pictures. In order to demonstrate the use of the photo-based 3D graphics modeling method in the real setting, a case study of modeling a precast façade on a building site is given.

3.3 PHOTO-BASED 3D MODELING OF SITE ELEMENTS: METHODOLOGY

Modeling the 3D construction graphics by photogrammetry concerns the transformation of 2D coordinates of a point on an object in the image plane into its 3D coordinates in the object space. The modeling method entails marking a limited quantity of feature points of the object on two photo images taken by one camera from two different locations. The camera’s position and orientation in the two shooting stations are analytically inferred from five paired feature points in the two pictures. The resulting equation systems suffice for solving the coordinates of any point on the object. The computing algorithms are given in detail as follows.

3.3.1 Two Photographs to Fix Spatial Point Position

The photogrammetry algorithm is based on definitions of the interior orientation and the exterior orientation of a photographic system. Fig. 3-1 gives a pinhole camera model to illustrate how a camera forms the image of a point on an object. The interior orientation is mainly described by the *principal point* and the *principal distance* of a camera. The *principal point* refers to the projected position of the perspective center (O in Fig. 3-1) on the image plane (x_o, y_o in Fig. 3-1) while the *principal distance* (c in Fig. 3-1) is the perpendicular distance between the perspective center and the image plane. To simplify calculation, the *principal distance* can be approximated as the focal length of the camera lens when the lens is focused at infinity, namely: $c \approx focal\ length$ (Poof given in Appendix I). The exterior orientation is defined by six parameters of the camera in the object coordinates system, namely, the three position coordinates of the camera's perspective center (X_o, Y_o, Z_o) plus the three Euler orientation angles (ω, ϕ, κ). The ω, ϕ, and κ are essentially the pitch, yaw, and roll angles of the camera, rotating around X, Y, and Z axes respectively in the object space as illustrated in Fig. 3-1.

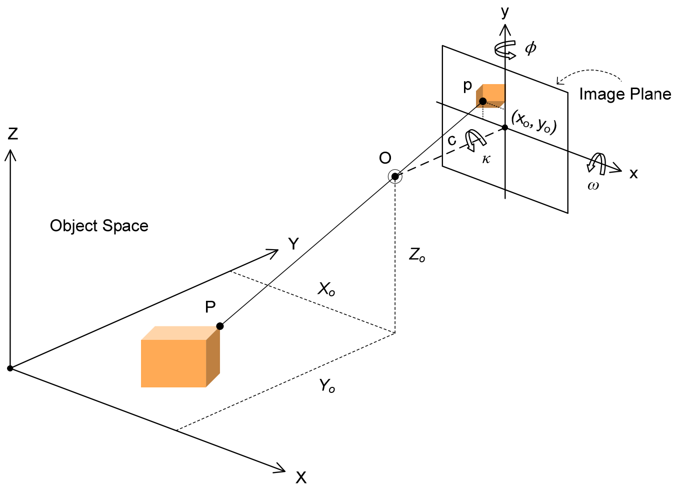

Fig. 3-1 Collinearity condition of spatial point *P*, camera perspective center *O*, and the image point *p* on the image plane

In the ideal situation, the spatial point *P*, the camera perspective center *O*, and its corresponding point *p* on the image plane are aligned along a straight line (Fig. 3-1). This yields a collinearity condition that the vector *Op* aligns with the vector *OP*, as given in Eq. (3-1):

$$\begin{bmatrix} X_n - X_o \\ Y_n - Y_o \\ Z_n - Z_o \end{bmatrix} = \lambda \boldsymbol{M}^T \begin{bmatrix} x_n - x_o \\ y_n - y_o \\ -c \end{bmatrix}. \tag{3-1}$$

The *Collinearity Equations* result from algebraic manipulation of Eq. (3-1) to unify the image coordinates system in the camera with the object coordinates system in the global space (Wong 1980; Wolf 1983; McGlone 1989), as given in Eq. (3-2) and Eq. (3-3):

$$
\begin{aligned}
X_n - X_o &= \lambda[m_{11}(x_n - x_o) + m_{21}(y_n - y_o) + m_{31}(-c)],\\
Y_n - Y_o &= \lambda[m_{12}(x_n - x_o) + m_{22}(y_n - y_o) + m_{32}(-c)],\\
Z_n - Z_o &= \lambda[m_{13}(x_n - x_o) + m_{23}(y_n - y_o) + m_{33}(-c)].
\end{aligned}
\tag{3-2}
$$

In Eq. (3-1) and Eq. (3-2), λ is a scale factor, c is the principal distance, and m_{ij} (i, j = 1, 2, 3) are the elements of a rotation matrix $\boldsymbol{M}$, which are expressed as functions of the Euler orientation angles (ω, ϕ, κ), as elaborated in Eq. (3-3):

$$
\begin{aligned}
m_{11} &= \cos\phi\cos\kappa,\\
m_{12} &= \sin\omega\sin\phi\cos\kappa + \cos\omega\sin\kappa,\\
m_{13} &= -\cos\omega\sin\phi\cos\kappa + \sin\omega\sin\kappa,\\
m_{21} &= -\cos\phi\sin\kappa,\\
m_{22} &= -\sin\omega\sin\phi\sin\kappa + \cos\omega\cos\kappa,\\
m_{23} &= \cos\omega\sin\phi\sin\kappa + \sin\omega\cos\kappa,\\
m_{31} &= \sin\phi,\\
m_{32} &= -\sin\omega\cos\phi,\\
m_{33} &= \cos\omega\cos\phi.
\end{aligned}
\tag{3-3}
$$

Eq. (3-2) analytically links the coordinates (x_n, y_n) of an image point on the image plane with its coordinates (X_n, Y_n, Z_n) in the global space. Given all the parameters of a camera are known, namely, c, (x_o, y_o), plus (X_o, Y_o, Z_o) and (ω, ϕ, κ) for the two camera stations, any spatial point can be fixed by intersecting two lines of light that are projected from two different camera stations (Fig. 3-2). Thus, with two pictures taken from two different camera stations, it is possible to calculate the coordinates of a point in the object coordinate system (X_n, Y_n, Z_n) from the coordinates of the point in the image coordinate system (x_n, y_n). Eventually, a collection of the points on the object, which are fixed by photogrammetry computing, suffice to produce a skeleton model of the object in 3D.

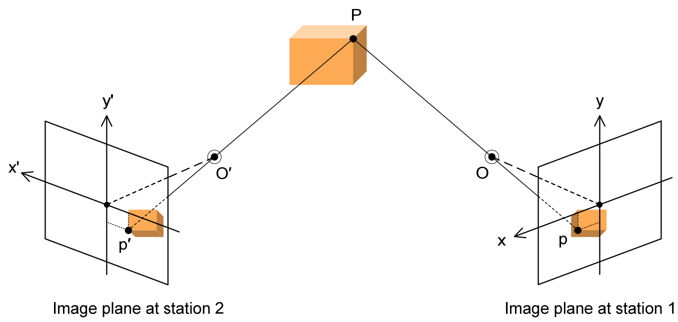

Fig. 3-2 Fixing the spatial point *P* on the object by intersecting two lines of sight from two camera stations

3.3.2 Coplanarity Equation

The camera's internal parameters (c, x_o, y_o) and external parameters (X_o, Y_o, Z_o, ω, ϕ, κ) at each station must be known before *collinearity equations* (Eq. 3-2) can be utilized to compute the spatial point coordinates. The internal parameters can be determined by camera calibrations or referring to the camera manufacturer's specifications. To determine the six external parameters, an analytical camera orientation method is proposed to calculate the positional displacement and relative rotation angles between the two camera stations. Put it in simple words, as shown in Fig. 3-2, the position and orientation of the camera station II on the left hand side will be computed relative to the camera station I on the right hand side.

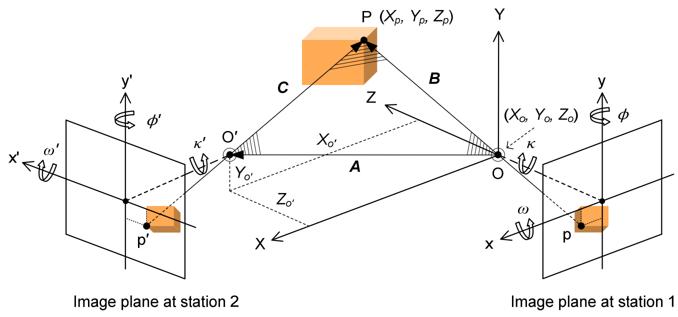

Fig. 3-3 Coplanarity condition of perspective centers *O*, *O′* and the spatial point *P*

Fig. 3-3 illustrates the two camera stations for shooting a point *P*, and a coplanar condition is formed by connecting the perspective center *O*, the perspective center *O'*, and the spatial point *P*. In this approach, we assume (X_o, Y_o, Z_o, ω, ϕ, κ) are the exterior orientation parameters of camera station I and ($X_{o'}$, $Y_{o'}$, $Z_{o'}$, ω', ϕ', κ') are those of camera station II. Then we define the vector ***A*** by connecting the point *O* to the point *O'*, ***B*** from the point *O* to the point *P*, and ***C*** from the point *O'* to the point *P* (Fig. 3-3). The vectors ***A***, ***B***, and ***C*** are bounded by a coplanar condition. Thus, their scalar triple product is equal to zero, which can be mathematically represented as a determinant in Eq. (3-4):

$$\boldsymbol{A}\cdot(\boldsymbol{B}\times\boldsymbol{C}) = \begin{vmatrix} X_{o'}-X_o & Y_{o'}-Y_o & Z_{o'}-Z_o \\ X_p-X_o & Y_p-Y_o & Z_p-Z_o \\ X_p-X_{o'} & Y_p-Y_{o'} & Z_p-Z_{o'} \end{vmatrix} = 0. \tag{3-4}$$

To remove the unknown spatial coordinates (X_p, Y_p, Z_p) of point *P* in Eq. (3-4), the *collinearity equations* (Eq. 3-2) are instantiated at the point *P* with its image coordinates associated with camera stations I and II being (x_p, y_p) and (x'_p, y'_p) respectively, yielding:

$$\begin{vmatrix} X_{o'} - X_o & Y_{o'} - Y_o & Z_{o'} - Z_o \\ m_{11}(x_p - x_o) + m_{21}(y_p - y_o) & m_{12}(x_p - x_o) + m_{22}(y_p - y_o) & m_{13}(x_p - x_o) + m_{23}(y_p - y_o) \\ +m_{31}(-c) & +m_{32}(-c) & +m_{33}(-c) \\ m'_{11}(x'_p - x_o) + m'_{21}(y'_p - y_o) & m'_{12}(x'_p - x_o) + m'_{22}(y'_p - y_o) & m'_{13}(x'_p - x_o) + m'_{23}(y'_p - y_o) \\ +m'_{31}(-c) & +m'_{32}(-c) & +m'_{33}(-c) \end{vmatrix} = 0. \quad (3\text{-}5)$$

Eq. (3-5) is also written in a form of determinant, in which the coplanar condition of ***A***, ***B*** and ***C*** is formulated in terms of the image coordinates of a spatial point *P* and the parameters of exterior orientations of the two camera stations only. Eq. (3-5) is commonly referred to as the *coplanarity equation* (Wong 1980; Wolf 1983).

To further simplify the formulation, the parameters of exterior orientations of the two camera stations in Eq. (3-5) are given in "relative" terms: the camera station I is arbitrarily taken as the origin, so (X_o, Y_o, Z_o, ω, ϕ, κ) can be all set to zero. In addition, $X_{o'}$ in connection with camera station II is used to fix the absolute scale of the object space. Hence, the remaining unknowns to be solved are only the five parameters of camera station II, namely, ($Y_{o'}, Z_{o'}, \omega', \phi', \kappa'$). Note here $Y_{o'}, Z_{o'}$ are relative coordinates scaled by $X_{o'}$; and $X_{o'}$ can be simply denoted by 1 or -1, depending on the camera station II being at the positive or negative side of x-axis of the image coordinate system inside the camera station I. Thus, there are five unknowns to be desired. Given (X_o, Y_o, Z_o, ω, ϕ, κ) are assumed (0, 0, 0, 0, 0, 0), Eq. (3-5) can be simplified as:

$$F = \begin{vmatrix} X_{o'} & Y_{o'} & Z_{o'} \\ x_p - x_o & y_p - y_o & -c \\ u & v & w \end{vmatrix} = 0. \quad (3\text{-}6)$$

where

$$\begin{aligned} u &= m'_{11}(x'_p - x_o) + m'_{21}(y'_p - y_o) + m'_{31}(-c), \\ v &= m'_{12}(x'_p - x_o) + m'_{22}(y'_p - y_o) + m'_{32}(-c), \\ w &= m'_{13}(x'_p - x_o) + m'_{23}(y'_p - y_o) + m'_{33}(-c). \end{aligned} \tag{3-7}$$

3.3.3 Five Pairs of Image Points to Determine Camera Positioning

Finding the direct solution to the *coplanarity equation* (Eq. 3-6) is difficult due to its inherent non-linearity. An alternative to tackling the *coplanarity equation* is by transforming the non-linear equations into linear equations and applying an iterative procedure to search for the most acceptable result (McGlone et al. 2004).

The linearization can be done by utilizing the Taylor series to expand the coplanarity condition equation and retain only the zero- and first-order terms, resulting in Eq. (3-8):

$$F = F_0 + \frac{\partial F}{\partial \boldsymbol{X}} \Delta \boldsymbol{X} = 0. \tag{3-8}$$

where

F_0 is the result of the function F evaluated with the approximate values of the five unknowns (initial values in the iterative procedure);

$\frac{\partial F}{\partial \boldsymbol{X}}$ is a row vector composed of the partial derivatives of F with respect to the five unknowns, of which the detailed expansions are given in Appendix II:

$$\frac{\partial F}{\partial \boldsymbol{X}} = \left[\frac{\partial F}{\partial Y_{o'}} \quad \frac{\partial F}{\partial Z_{o'}} \quad \frac{\partial F}{\partial \omega'} \quad \frac{\partial F}{\partial \phi'} \quad \frac{\partial F}{\partial \kappa'} \right], \tag{3-9}$$

and $\Delta \boldsymbol{X}$ is a column vector composed of the corrections to the five unknowns:

$$\Delta \boldsymbol{X} = \left[\Delta Y_{o'} \quad \Delta Z_{o'} \quad \Delta \omega' \quad \Delta \phi' \quad \Delta \kappa' \right]^T. \tag{3-10}$$

For n feature points, their paired image coordinates in two respective picture frames are plugged into Eq. (3-8) to form n sets of coplanarity condition equations, which can be compactly represented in the matrix form as Eq. (3-11):

$$\underset{n\times 1}{\boldsymbol{F_0}} + \underset{n\times 5}{\frac{\partial \boldsymbol{F}}{\partial \boldsymbol{X}}} \underset{5\times 1}{\Delta \boldsymbol{X}} = \underset{n\times 1}{\mathbf{0}}. \tag{3-11}$$

Thus, a minimum of five image points (n = 5) are theoretically sufficient to calculate the vector of the corrections $\Delta \boldsymbol{X}$ by:

$$\underset{5\times 1}{\Delta \boldsymbol{X}} = (\underset{5\times 5}{\frac{\partial \boldsymbol{F}}{\partial \boldsymbol{X}}})^{-1} (-\underset{5\times 1}{\boldsymbol{F_0}}). \tag{3-12}$$

An iterative procedure can be performed on Eq. (3-12) starting with initial approximations (***X₀***) of the five unknowns in searching for the minimum of the corrections ($\Delta \boldsymbol{X}$). The initial approximations ($\boldsymbol{X_0}$) are input into Eq. (3-12) to calculate the corrections ($\Delta \boldsymbol{X_1}$) of the first iteration. Then $\Delta \boldsymbol{X_1}$ is added to $\boldsymbol{X_0}$ to yield the incremental approximations as $\boldsymbol{X_1} = \boldsymbol{X_0} + \Delta\boldsymbol{X_1}$. $\boldsymbol{X_1}$ is used as the input to calculate the corrections ($\Delta\boldsymbol{X_2}$) for the second iteration. The iterative procedure loops until the corrections ($\Delta\boldsymbol{X_n}$) become increments with negligible magnitudes, satisfying the threshold of desired accuracy. The solution of the five unknowns accordingly gives the approximate solution ($\boldsymbol{X_n}$) at the *n*th iteration where the iterative procedure stops.

3.3.4 Least Squares Adjustment

In practice, it is commonplace that there are more than five points on two photos readily available for image data processing. To achieve more statistically significant and reliable solutions by taking full advantage of all the points available (n > 5), the least squares adjustment method can be applied. The "least squares" principle is to minimize the sum of the squares of the residuals on all the available points, formulated in Eq. (3-13) (Mikhail 1976):

$$\phi = \sum_{i=1}^{n} (v_i^2) = \boldsymbol{v}^T \boldsymbol{v} \rightarrow \min. \tag{3-13}$$

where $\boldsymbol{v} = \begin{bmatrix} v_1 & v_2 & \dots & v_n \end{bmatrix}^T$ is the column vector of residuals on the n observations of the *coplanarity equations*. With the residuals $\boldsymbol{v}$ added, the matrix of the linearized *coplanarity equations* (Eq. 3-11) can be rewritten as Eq. (3-14):

$$\underset{n\times1}{\boldsymbol{v}} + \underset{n\times1}{\boldsymbol{F_0}} + \underset{n\times5}{\frac{\partial \boldsymbol{F}}{\partial \boldsymbol{X}}} \underset{5\times1}{\Delta\boldsymbol{X}} = \underset{n\times1}{\boldsymbol{0}}. \tag{3-14}$$

Thus the scalar to be minimized in Eq. (3-13) is:

$$\begin{aligned}\phi &= \boldsymbol{v}^T\boldsymbol{v}\\ &= (-\boldsymbol{F_0} - \frac{\partial \boldsymbol{F}}{\partial \boldsymbol{X}}\Delta \boldsymbol{X})^T(-\boldsymbol{F_0} - \frac{\partial \boldsymbol{F}}{\partial \boldsymbol{X}}\Delta \boldsymbol{X})\\ &= (\Delta \boldsymbol{X})^T(\frac{\partial \boldsymbol{F}}{\partial \boldsymbol{X}})^T\frac{\partial \boldsymbol{F}}{\partial \boldsymbol{X}}\Delta \boldsymbol{X} + 2(\boldsymbol{F_0})^T\frac{\partial \boldsymbol{F}}{\partial \boldsymbol{X}}\Delta \boldsymbol{X} + (\boldsymbol{F_0})^T\boldsymbol{F_0}.\end{aligned} \quad (3\text{-}15)$$

Taking partial derivatives on Eq. (3-15) with respect to the free variables of the column vector $\Delta \boldsymbol{X}$ and equating them to zero, we have Eq. (3-16):

$$\frac{\partial \phi}{\partial(\Delta \boldsymbol{X})} = 2(\Delta \boldsymbol{X})^T(\frac{\partial \boldsymbol{F}}{\partial \boldsymbol{X}})^T\frac{\partial \boldsymbol{F}}{\partial \boldsymbol{X}} + 2(\boldsymbol{F_0})^T\frac{\partial \boldsymbol{F}}{\partial \boldsymbol{X}} = \mathbf{0}. \quad (3\text{-}16)$$

Transposing Eq. (3-16) and rearranging it as Eq. (3-17):

$$[(\frac{\partial \boldsymbol{F}}{\partial \boldsymbol{X}})^T\frac{\partial \boldsymbol{F}}{\partial \boldsymbol{X}}]\Delta \boldsymbol{X} = -(\frac{\partial \boldsymbol{F}}{\partial \boldsymbol{X}})^T\boldsymbol{F_0}. \quad (3\text{-}17)$$

We finally derive the corrections (the elements of $\Delta \boldsymbol{X}$) to the five unknowns to be desired in Eq. (3-18):

$$\underset{5\times 1}{\Delta \boldsymbol{X}} = -[(\underset{5\times n}{\frac{\partial \boldsymbol{F}}{\partial \boldsymbol{X}}})^T\underset{n\times 5}{\frac{\partial \boldsymbol{F}}{\partial \boldsymbol{X}}}]^{-1}(\underset{5\times n}{\frac{\partial \boldsymbol{F}}{\partial \boldsymbol{X}}})^T\underset{n\times 1}{\boldsymbol{F_0}}. \quad (3\text{-}18)$$

The same iterative procedure can be applied on Eq. (3-18) to search for the most probable estimates about the five unknown parameters of camera station II ($Y_{o'}, Z_{o'}, \omega', \phi', \kappa'$). The following section uses a simplest "box" to illustrate the computation procedure of the established modeling method.

3.3.5 Calculation Example

A simple cubic box is used to illustrate the photo-based analytical 3D modeling approach. The box is photographed with one digital camera sequentially from two stations (Fig. 3-4). The camera station profiled with red line is referred to as the camera station I.

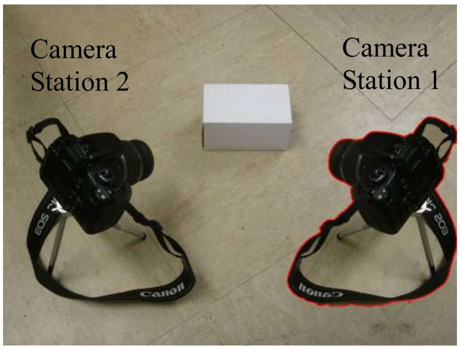

Fig. 3-4 Photographing the cubic box from camera stations

In this example, the six points on the box's six corners are marked on the two photos and their 2D coordinates in the photo image frames provide the input to calculate the camera exterior parameters (Fig. 3-5). In Fig. 3-5, the photo image frame is defined with x, y axes pointing rightward and downward respectively; and the marked points are tagged with Arabic numerals to show the correspondence relationship of paired points between the two photos.

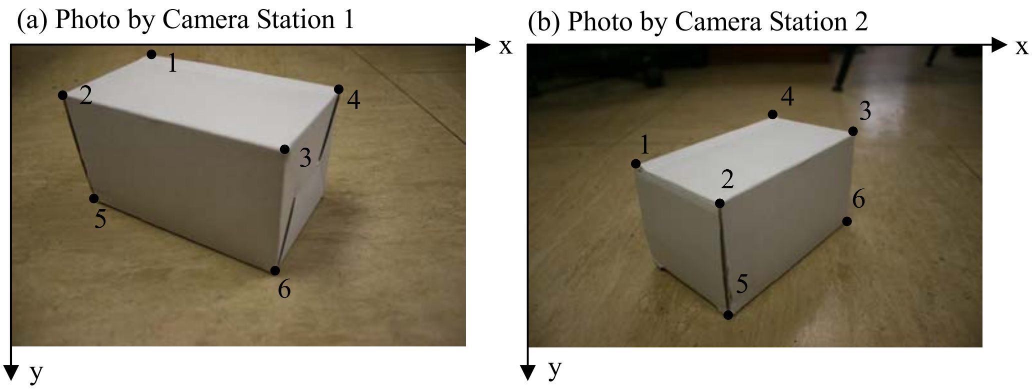

Fig. 3-5 Two captured photos with six paired points marked

Table 3-1 records the coordinates of all the marker points in pixels. They are further transformed into metrics in the camera image plane. According to the camera specification (Canon Eos 400D), the CCD size is 22.2 × 14.8 mm and the image resolution is 3888 × 2592 pixel. Thus, the transformation equations are $x_m = \frac{22.2}{3888} \times x_p$ and $y_m = 14.8 - \frac{14.8}{2592} \times y_p$ for the x, y axes respectively. Table 3-2 shows the transformed coordinates of the marked points in millimeters.

Table 3-1 Coordinates of marker points in pixels

Marker No.	Photo 1 (pixel)		Photo 2 (pixel)	
	x_p	y_p	x_p	y_p
1	432.5	440	1644	1367
2	2346	943	2796	759
3	2811	389.5	2117.5	607.5
4	1182	93	916	1041
5	725	1344.5	1729	2313
6	2251	1984	2730	1510

Table 3-2 Transformed coordinates of marker points on camera image planes

Marker No.	Photo 1 (mm)		Photo 2 (mm)	
	x_m	y_m	x_m	y_m
1	2.470	12.288	9.387	6.995
2	13.395	9.416	15.965	10.466
3	16.051	12.576	12.091	11.331
4	6.749	14.269	5.230	8.856
5	4.140	7.123	9.872	1.593
6	12.853	3.472	15.588	6.178

The six pairs of image coordinates are further utilized to calculate the relative exterior orientations of the two camera stations. The camera station I is fixed as the reference frame system (0, 0, 0, 0, 0, 0); since the number of the *coplanarity equations* constructed (n = 6) is larger than five, the iterative procedure of least squares adjustment is applied on Eq. (3-18) to search for the desired five unknowns, yielding the relative position and orientation of the camera station II as (-1.000, 0.360, -0.427, -27.420°, -59.737°, -63.952°). Note, the scale factor $X_{o'}$ of the camera station II is determined as minus one (-1), as the camera station II is on the negative side of x-axis of the picture frame associated with the camera station I. For practical calculation, the $X_{o'}$ can be either plus one or minus one as a result of evaluating the two possible solutions for the position and orientation of the camera station II. Then, any object point can be used to determine the valid solution, as such the object point should be located in front of both of the camera stations.

The camera interior configurations are given as: focal length: f = 18 mm, principal point: x_o = 11.1 mm, y_o = 7.4 mm. Plugging them together with the calculated exterior orientations into Eq. (3-2), we obtain four polynomials:

$$
\begin{aligned}
&X_n + \frac{(x_n - 11.1)}{18} Z_n = 0, \\
&Y_n + \frac{(y_n - 7.4)}{18} Z_n = 0, \\
&X_n + \frac{0.2213x_n^{'} + 0.4528y_n^{'} + 9.7395}{0.7504x_n^{'} + 0.4866y_n^{'} - 19.9835} Z_n + \frac{0.8449x_n^{'} + 0.6799y_n^{'} - 15.8247}{0.7504x_n^{'} + 0.4866y_n^{'} - 19.9835} = 0, \\
&Y_n + \frac{-0.6228x_n^{'} + 0.7471y_n^{'} - 2.7933}{0.7504x_n^{'} + 0.4866y_n^{'} - 19.9835} Z_n + \frac{-0.5361x_n^{'} + 0.1438y_n^{'} + 6.0013}{0.7504x_n^{'} + 0.4866y_n^{'} - 19.9835} = 0.
\end{aligned}
\tag{3-19}
$$

where x_n, y_n denote the image coordinates in photo 1 and $x_n^{'}$, $y_n^{'}$ denote those in photo 2.

As such, any object point can be computed by Eq. (3-19) based on the corresponding image coordinates on the two photos. The least-squares adjustment is recommended since the quantity of polynomial equations (four) is greater than three - that is the quantity of the desired unknowns (X_n, Y_n, Z_n). The spatial coordinates of the six marker points are calculated as shown in Table 3-3, based on which, the cubic box is precisely modeled in 3D. Two snapshots of the model in the same perspectives as the two photos taken are shown in Fig. 3-6.

Table 3-3 Calculated spatial coordinates of six marker points (dimensionless)

Marker No.	X_n	Y_n	Z_n
1	-0.391	0.221	-0.815
2	0.076	0.067	-0.601
3	0.221	0.231	-0.802
4	-0.248	0.389	-1.020
5	-0.387	-0.016	-0.999
6	0.076	-0.171	-0.782

(a) Model view by Camera Station 1 (b) Model view by Camera Station 2

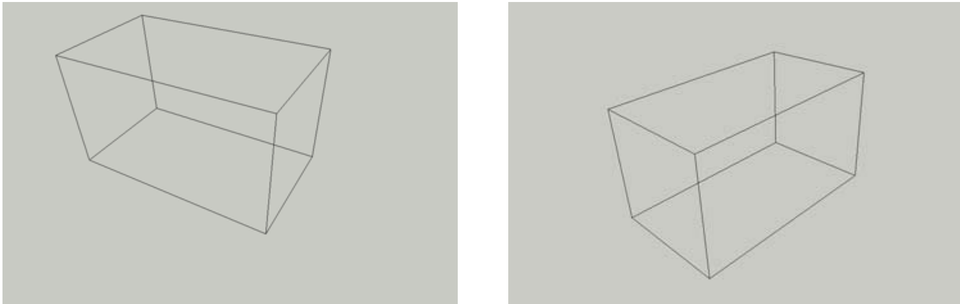

Fig. 3-6 Views of the 3D box model from the same perspectives as two photos were taken

3.4 CASE STUDY: MODELING PRECAST FAÇADE ON SITE

This case study models a precast facade at a building site to further verify the feasibility of the photo-based modeling method being proposed and demonstrate the application of the method in a practical setting. On a construction site, precast building elements often feature relative complex configurations and bulky sizes. This requires more than two photos to be taken in order to reveal sufficient features of the building element. Therefore, a sequence of site photos taken from different angles are analyzed two at a time in order to determine the positions and orientations of multiple sequential camera stations. In particular, we shed light on how to unite the scales of the object in two different object spaces formed by three consecutive photos, illustrated with the case of a precast façade.

3.4.1 Taking Photos on Site

A practical construction site differs substantially from an ideal laboratory environment, presenting numerous constraints on taking photos in terms of accessibility, line-of-sight, and lighting. A precast façade with relatively complex design features was selected on a residential building project in Hong Kong. Fig. 3-7 shows the frontal face of the facade featuring an alcove window.

Fig. 3-7 The precast façade being modeled

In this experiment, a digital single lens reflection (DSLR) camera (Canon EOS 400D) was used, with its focal length fixed at 18 mm to obtain the widest shooting scope of the lens. When taking photos on site, it is preferable that each feature point of the facade should be covered in three or more photos so as to facilitate follow-up analysis. Generally, three different camera stations would suffice to photograph a convex face of an object; as for an alcove in the object (e.g., the frontal face of the façade), usually two extra camera stations are recommended to cover the four inner corners of the alcove. Thus, according to the above guideline, in modeling the precast façade on site, it would be ideal to have eight photos to capture the four convex faces and two additional photos to cover the alcove window in the frontal face.

However, it is worth mentioning that not all the photos as desired could be successfully acquired due to obstructions of line of sight and inaccessibility to some shooting stations on site. In the current case, the surrounding area at the rear face of the façade was relatively open while its frontal face was close to another facade laid in a row. As such, there was limited room for placing the camera stations to photograph the frontal face as well as the alcove window on the site. Instead of the ten photos as planned, we managed to shoot eight pictures as shown in Fig. 3-8 according to the photo-taking sequence on site.

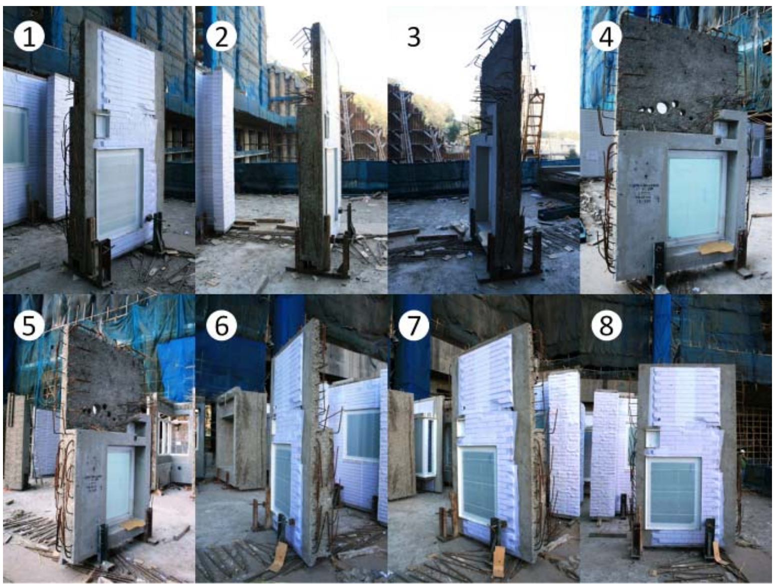

Fig. 3-8 Eight precast façade photos sequentially taken on the building site

3.4.2 Modeling Facade

Sufficient marker points on the façade were identified in those photos taken from the site in order to determine the external parameters of the eight camera stations and calculate the spatial coordinates of those marker points. In calculating the relative orientations of eight camera stations, the Y coordinate of each camera station was chosen as the scale factor instead of taking X-axis, as all the eight photos were taken in "portrait" frames.

Similar to the cubic box example, nine points were marked on photo 1 and photo 2 (the white dots annotated with No. 1~9 in Fig. 3-9). The *coplanarity equations* and least squares adjustment were applied to compute the relative positions and orientations between the camera stations 1 and 2, and the resulting *collinearity equations* were subsequently evaluated to calculate the spatial coordinates of the nine points on the façade.

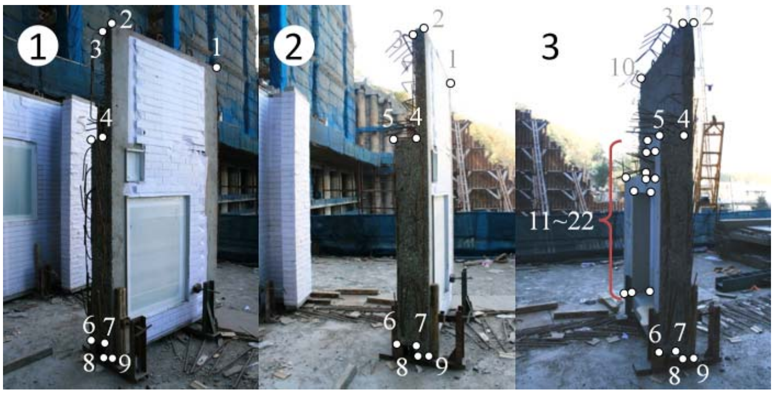

Fig. 3-9 Three consecutive photos 1, 2, and 3 with feature points of the façade marked and numbered

The next step is to use the established camera station 2 to determine the position and orientation of the camera station 3. In Fig. 3-9, the photo 3 shares eight common points (No. 2~9) with photo 2. The same procedure was repeated to determine the relative orientation of camera station 3. Note, the camera station 2 is initialized with the position coordinates (0, 0, 0) and the orientation angles (ω_2, ϕ_2, κ_2), where the (ω_2, ϕ_2, κ_2) are the relative orientation angles of camera station 2 with respect to camera station 1.

It's noted that the scales of the object coordinate system where camera stations 1 and 2 reside (denoted by $I_{1\text{-}2}$) may not be the same as the one where camera stations 2 and 3 reside (denoted by $I_{2\text{-}3}$). A *scale transfer* operation should be conducted to make the scales of two coordinate systems agreeable (Moffitt and Mikhail 1980). The *scale transfer* is performed as follows: (1) calculating the average distances $\bar{d}$ and $\bar{d}'$ from the perspective center of camera station 2 to all the "triple overlap" points (No. 2 ~ 9) in $I_{1\text{-}2}$ and $I_{2\text{-}3}$ respectively; (2) then obtaining the scale factor $\alpha = \bar{d} / \bar{d}'$; (3) using the scale factor α to synchronize the coordinates of the camera station 3: $\boldsymbol{X}_{o_3} = \boldsymbol{X}_{o_2} + \alpha \boldsymbol{X}'_{o_3}$, where the vectors $\boldsymbol{X}_{o_2}$ and $\boldsymbol{X}_{o_3}$ are the spatial coordinates of camera station 2 and camera station 3 in $I_{1\text{-}2}$, and $\boldsymbol{X}'_{o_3}$ are those of camera station 3 in $I_{2\text{-}3}$. As such, the position and orientation of the camera station 3 can be defined in the object coordinate system where the camera stations 1 and 2 reside.

On photo 3, there are thirteen additional marker points (No. 10~22). These points together with the other points (No. 2~9) would be used to calculate the external parameters of the successive camera station 4. Repeating the aforementioned procedures, all eight camera stations can be fixed. Table 3-4 gives all the positions and orientations of the eight camera stations. Using the information in Table 3-4, the coordinates of the marker points on the precast façade are subsequently computed and the precast façade model is built as shown in Fig. 3-10.

Table 3-4 Relative positions and orientations of eight camera stations

Camera Station No.	Position (dimensionless)			Orientation (degree)		
	X	Y	Z	α	ϕ	κ
1	0.000	0.000	0.000	0.000	0.000	0.000
2	-0.008	1.000	-0.219	-26.778	-0.330	0.078
3	-0.011	1.563	-0.937	-58.713	-0.325	1.612
4	0.016	0.472	-3.423	-155.791	-0.381	-0.100
5	0.028	-0.267	-3.884	179.203	-1.749	-0.485
6	0.068	-2.090	-2.587	108.177	0.044	0.241
7	0.092	-2.178	-1.904	90.514	0.316	-1.430
8	0.165	-1.701	-0.278	44.846	-0.896	0.896

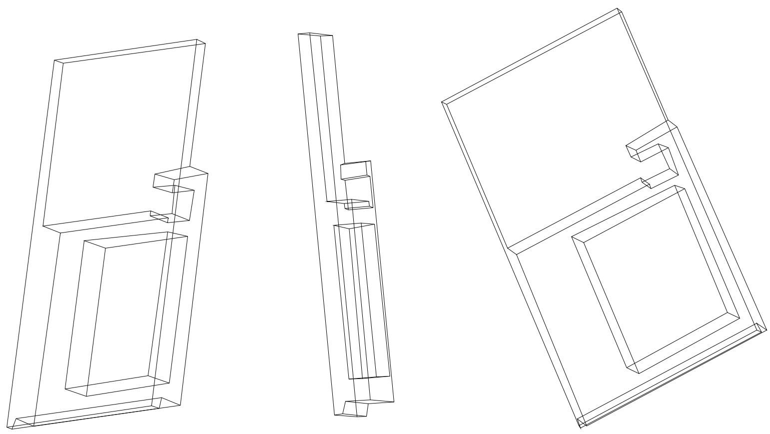

Fig. 3-10 Views of the 3D façade model from different perspectives

3.5 SUMMARY

This chapter establishes a 3D construction modeling method based on the mechanism of photogrammetry, which analytically processes the image data contained in site photos into a 3D model of a site element. Differing from conventional computer-aided design (CAD) or virtual reality (VR) modeling, the proposed method takes advantage of the site photos easily acquired with a digital camera to build 3D models for site elements. Rather than using surveying instruments, the proposed method resorts to a minimum of five pairs of image points on the object from two photos taken at two different camera stations in order to determine the positions and orientations of the two camera stations. With more than five paired image points available, the least squares adjustment is utilized to produce the most probable modeling results. The mathematical formulas established have been verified in a simple “box” example.

To further demonstrate the feasibility of the proposed method in practical settings, a case study of modeling a precast façade on a building site is given. The precast façade features relative complex configurations and bulky sizes. This requires more than two photos to be taken in order to reveal sufficient features of the building element. Eight site photos taken from different angles were analyzed in order to determine the positions and orientations of multiple camera stations and calculate the spatial coordinates of all the feature points. In particular, we shed light on how to unite the scales of the object in two different object spaces formed by three consecutive camera stations.

In conducting site experiments, we encountered practical constraints for taking site photos and implementing the proposed method. They are summarized as below:

- Obstacles may get in the way between the camera and the object. This may block the line of sight for certain feature points, causing loss of information in the photo. For example, temporary supporting rigs make some edges or corners invisible in one photo of the facade.

- Appropriate shooting perspectives from particular camera stations may not be available on a congested site. For example, the camera was not allowed to be placed in an inaccessible area; or the rear face of the building element could be only photographed at a neighboring residential building that was inaccessible.

- Tradeoff between the shooting scope and the detail of photo. When taking pictures with a camera with a fixed focal length (required for photogrammetry analysis), the modeler may need to resolve the tradeoff between staying far away from the object to obtain a wide scope of content and getting a “close-up” view of the object in order to grasp granular details.

- Marking feature points on the object in different photos demands precision and patience on the modeler. In future research, development of algorithms for automatically identifying the same feature points in different photos will further enhance the proposed method.

The proposed photo-based modeling method may suffer from two types of modeling errors: (1) the systematic error due to camera lens distortions and (2) the random error due to human factors, which will be addressed in detail in the next chapter. The systematic error may cause the image point, which is projected from the object space onto the camera image plane, to shift from its true position to a perturbed position in the image plane. The human error refers to the discrepancy between the true position of a feature point in a photo and the position of a point the modeler actually selects. Thus, it is recommended that more than two photos are taken to capture each feature point on the target object such that the least squares adjustment can be applied to enhance the modeling accuracy in practical applications. In such a way, the most probable values of the coordinates of each feature point on the object can be deduced and the 3D model of the object can be generated to support critical applications in construction management such as quantity surveying on as-built models, dimension checking on prefabricated elements for quality control, and visualization of project progress and site operations.

CHAPTER 4

ASSESSING ACCURACY OF APPLYING PHOTOGRAMMETRY TO TAKE GEOMETRIC MEASUREMENTS ON BUILDING PRODUCTS

4.1 INTRODUCTION

This chapter characterizes the errors of the photogrammetry-derived geometric measurements on building products in a systematic, practical and statistically significant way. In this research, we intend to use the off-the-shelf, portable digital cameras, instead of high-end, expensive cameras specially manufactured for photogrammetry applications. Our research falls into the category of close-range photogrammetry measurement, which usually applies to those situations where the target object is away from the camera at a distance ranging from 1 m to 300 m (Luhmann et al. 2006). We further narrow the shooting range to [1m, 6m] so to be aligned with practical application needs for quantity surveying in building construction. The application setting is given as follows:

A site engineer is responsible for taking geometric measurements on building products that have been just placed or partially completed. Those measurements represent the as-built information and are used (1) to ascertain the actual quantity of work completed, (2) to check the quality of finished products against the building design and technical specifications, and (3) to certify payment requests filed by the contractor. In the conventional way, the engineer would apply a measurement tape to determine the length of each dimension of a building product and record the data in a form and on the spot.

As an alternative, the engineer simply takes snapshots of the building product with a digital camera from different angles. Back in office, the engineer derives as-built measurements through post processing those photos by use of photogrammetry software. In addition, applying the photogrammetry method at a building site would produce two "by-product" benefits: First, measurements can be taken effortlessly on those building elements situated in hazardous areas that are unsafe to access. Second, the alignment of a building product can be continuously monitored by taking site pictures at different times.

The remainder of this chapter is organized as follows: The major reasons that account for errors in the geometric measurements obtained by photogrammetry are first explained; they are (1) the systematic error due to distortion of the camera lens and (2) the random error due to human factors. Then, we describe the steps of method application, experiment design, and the sample data acquired. After revealing biases and limitations of applying regression and correlation coefficient methods for error analysis, we resort to the 95% limits of agreement method to assess the accuracy of photogrammetry based on the sample data. We further establish the confidence intervals for the limits of agreement in order to ensure validity and statistical significance of the results. The practical implication and applicability of the photogrammetry-based approach to construction engineering applications is discussed before drawing conclusions.

4.2 INDUCED PHOTOGRAMMETRIC ERRORS

In this section, we discuss two major factors that induce the measurement errors of photogrammetry.

4.2.1 Systematic Error due to Lens Distortion

Measurement errors due to camera lens distortion can be treated as the systematic error with a consistent effect (Viswanathan 2005). It causes an image point on the image plane to shift from its true position (x_n', y_n') to a perturbed position (x_n, y_n). Thus, the true coordinates of any image point can be compensated by Eq. (4-1):

$$\begin{aligned} x_n' &= x_n + dx, \\ y_n' &= y_n + dy. \end{aligned} \tag{4-1}$$

The camera lens distortion (i.e. *dx* and *dy*) can be taken as the aggregate of the radial distortion and the decentering distortion (Beyer et al. 1995; Fraser 1996). As the lens of a camera is actually composed of a combination of lenses, the centers of those lens elements are not strictly collinear, giving rise to decentering distortion. In contrast, the radial distortion occurs in each single optical lens and the distortion effect is magnified along the radial direction of the lens: the further a point is away from the center of the lens, the larger error is produced for its projected image point. Therefore, dx, dy can be decomposed by Eq. (4-2):

$$\begin{aligned} dx &= dx_r + dx_d, \\ dy &= dy_r + dy_d. \end{aligned} \tag{4-2}$$

Assuming the optical axis of the lens is perpendicular to the image plane, the lens distortion can be further modeled by Eq. (4-3) that was developed by Brown (1966):

$$\begin{aligned} dx_r &= K_1(x_n - x_p)r^2 + K_2(x_n - x_p)r^4, \\ dy_r &= K_1(y_n - y_p)r^2 + K_2(y_n - y_p)r^4, \\ dx_d &= P_1[r^2 + 2(x_n - x_p)^2] + 2P_2(x_n - x_p)(y_n - y_p), \\ dy_d &= P_2[r^2 + 2(y_n - y_p)^2] + 2P_1(x_n - x_p)(y_n - y_p), \\ r^2 &= (x_n - x_p)^2 + (y_n - y_p)^2. \end{aligned} \tag{4-3}$$

Here x_p and y_p are the coordinates of the principal point, K_1 and K_2 are the radial distortion parameters, and P_1 and P_2 are the decentering distortion parameters. When the lens distortion is small, the systematic error due to the lens distortion can be ignored, namely, $x_n' \approx x_n$ and $y_n' \approx y_n$; otherwise, the systematic error should be corrected.

Those parameters (K_1, K_2, P_1, P_2) need to be first determined by following analytical procedures to calibrate the camera (Tsai 1987; Rüther 1989). In our research, we applied the software of PhotoModeler® to calibrate a Canon EOS 400D camera with its focal length fixed at 18 mm (K_1 is 5.167e-004, K_2 is -1.120e-006, P_1 is 3.924e-005, and P_2 is 3.684e-005) (detailed calibration procedure is included in Appendix III). The calibration results indicate the lens distortion of the camera is relatively small.

4.2.2 Random Error due to Human Factors

Theoretically, one point captured in two different photos is sufficient to fix its 3D coordinates. To complete this step requires identifying and marking the point in the two photos. Any human error in point marking gives rise to another form of error – the random error (Viswanathan 2005).

As shown in Fig. 4-1, we assume that the point of $P'(x', y')$ is the true position of a target point, whereas the point of $P_1(x_1, y_1)$ is fixed by photogrammetry computations. The discrepancy between the two points is attributed to imprecise point marking.

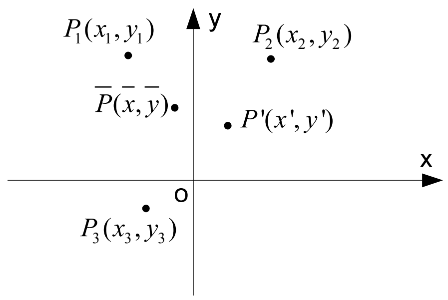

Fig. 4-1 Simple illustration of random error: various points' coordinates derived for one identical point

To reduce this error, it is advisable to include the target point in three or more photos. At the expense of redundancy, the random error on any of the photos can be compensated by the others. For example, if the target point is covered in three photos, then any two can be used to derive the point by photogrammetry, resulting in a total of three points *(P_1, P_2, P_3)* (Fig. 4-1). As the true position of $P'(x', y')$ actually is unknown, the most likely coordinates of the target point can be determined by least squares adjustment (Mikhail 1976), which minimizes the sum of the squares of the residuals as in Eq. (4-4):

$$\sum_{i=1}^{n}(v_i)^2 = (v_1)^2 + (v_2)^2 + \cdots + (v_n)^2 = \min. \tag{4-4}$$

where $v_1, v_2, \ldots, v_n$ are the residuals on the n measurements. Given our three-point example, we have Eq. (4-4a) for least squares adjustment.

$$\begin{aligned}\sum_{i=1}^{3}(v_{xi})^2 &= (x-x_1)^2 + (x-x_2)^2 + (x-x_3)^2, \\ \sum_{i=1}^{3}(v_{yi})^2 &= (y-y_1)^2 + (y-y_2)^2 + (y-y_3)^2.\end{aligned} \tag{4-4a}$$

Taking derivatives with respect to each unknown and equating them to zero, we have Eq. (4-4b):

$$\begin{aligned}\frac{d\sum_{i=1}^{3}(v_{xi})^2}{dx} &= 2(x-x_1) + 2(x-x_2) + 2(x-x_3) = 0, \\ \frac{d\sum_{i=1}^{3}(v_{yi})^2}{dy} &= 2(y-y_1) + 2(y-y_2) + 2(y-y_3) = 0.\end{aligned} \tag{4-4b}$$

Therefore, an approximation of the target point coordinates is as (4-4c):

$$\begin{aligned}\overline{x} = x &= \frac{x_1 + x_2 + x_3}{3}, \\ \overline{y} = y &= \frac{y_1 + y_2 + y_3}{3}.\end{aligned} \tag{4-4c}$$

The resulting $(\bar{x}, \bar{y})$, from a statistical perspective, is more reliable than any single point measured. Note, unlike the systematic error, the random error due to human factors cannot be analytically removed. In fact, our present research is mainly concerned with assessing the random error of photogrammetry in taking geometric measurements on building products.

4.3 EXPERIMENT DESIGN AND SAMPLE DATA

Our experiment designed for assessing the measurement error of photogrammetry includes the following six steps: (1) identifying a set of target objects, taking measurement of geometric dimensions by tape for each object, and recording measurement data, (2) taking sufficient photos of the same set of target objects by using a digital camera with fixed focal length, (3) processing photos into 3D representations of the target objects by using photogrammetry software, (4) fixing the scale of each object model by identifying a reference line, (5) taking geometric measurements on each object based on its 3D model, and (6) conducting accuracy analysis by comparing the two sets of measurements.

A photo-based 3D model resulting from the above step 3 only represents the relative scale of each edge on the object. To convert the relative scales into the absolute measurements requires determination of the length of a reference line in the absolute unit of measure. This reference line can be one edge on the object that can be easily measured by tape. In case that the target object is not accessible, the reference line can be taken by one edge of an adjacent object which can be spatially related with the current object. For instance, a concrete block sits on top of a tall platform; one edge on the platform is parallel to one edge of the concrete block. We can take the edge on the platform as the reference line, and include the platform in the photos of the concrete block. In this way, the absolute measures on all the edges of the concrete block can be fixed by photogrammetry.

The twelve objects sampled in our experiment were the building products and building facilities found on the campus of Hong Kong Polytechnic University. We simply took one edge on each object as the reference line for scaling purpose. Table 4-1 lists the sample data consisting of seventy-nine paired dimension measurements by tape and by photogrammetry respectively. Note, in Table 4-1, as the first measurement on each subject is used as the reference line for scaling, it is excluded from ensuing error analysis. Thus, the sample data available for error analysis consists of sixty-seven pairs of geometric measurements. It is noted that the sample size is statistically significant to the following measurement error analysis in consideration of the expected accuracy level being in the order of 1 cm and the relatively small variation on the measurement errors (the sample standard deviation of measurement error being 6.81 mm).

Table 4-1 Seventy-nine paired dimension measurements taken from twelve subjects by tape and by photogrammetry respectively

Subject name	Tape measurement (mm)	Photo-based measurement (mm)	Subject name	Tape measurement (mm)	Photo-based measurement (mm)
“Air conditioner”	*5720*	*5720*	“Power-transmission equipment”	*610*	*610*
	900	892		230	228
	1570	1577		270	264
	500	500		100	103
	2140	2125		100	102
	1300	1295		995	992
	150	146		990	992
	770	765		225	226
“Windows of classroom”	*2120*	*2120*	“Door of classroom”	*2520*	*2520*
	400	386		2050	2038
	130	129		2070	2071
	2120	2108		1470	1476
	1010	1001		35	38
	400	397		1090	1083
“Building entrance”	*370*	*370*	“Balcony”	*1980*	*1980*
	740	740		140	129
	1690	1683		1880	1874
	755	742		930	937
	290	288		340	339
“Road signboard”	*830*	*830*	“Ventilation equipment”	*870*	*870*
	180	179		147	145
	800	799		950	945
	1550	1551		600	605
	1550	1550		725	721
	150	149		145	144
	800	800		225	226
	150	150		955	950
“Jockey-hall signboard”	*2830*	*2830*	“Medals podium”	*350*	*350*
	655	659		1800	1796
	2730	2743		300	299
	1020	1022		350	352
	800	797		600	600
	800	784		300	299
	615	618		475	475
	275	294			
“Pavilion”	*690*	*690*	“Caution signboard”	*865*	*865*
	800	797		250	255
	685	658		75	76
	650	651		865	869
	650	651			
	740	736			

4.4 ANALYSIS OF PHOTOGRAMMETRY ACCURACY

4.4.1 Visual Assessment of Agreement

That two measurement methods agree with each other means they yield comparable, interchangeable results when applied on the same object. Fig. 4-2 contrasts photo-based measurements against tape readings based on our sample data. All sample points would lie on the line of equality (the diagonal line in Fig. 4-2), indicating the two sets of measurements agree with each other. However, when the range of variation on the measurements is large compared with the difference between the two sets of measurements, this plot may become obscure and inadequate to substantiate the agreement between the two sets of measurements (Bland and Altman 1999). Our case serves as an example: the geometric measurements in the sample data vary in meters (ranging from 0.75 m to 2.8 m) while the differences between the two sets of measurements only differ in millimeters (ranging from -10 mm to 20 mm).

A better way to visualize the agreement of data is to plot the difference between the two sets of measurements against zero, as given in Fig. 4-3. We can observe a good agreement between the two sets of measurements: the differences are enveloped within -10 mm to 20 mm, except for three outliers.

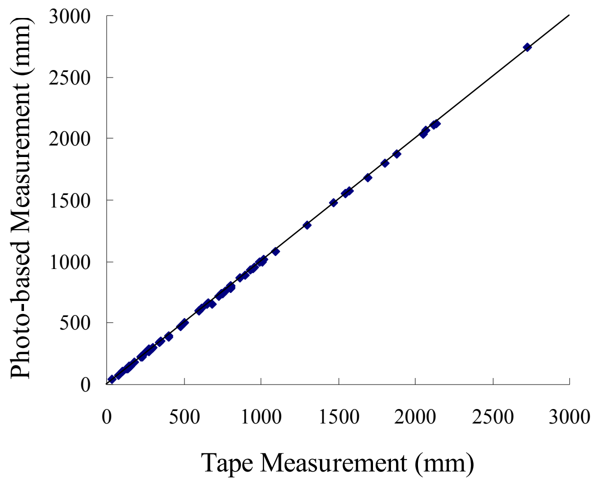

Fig. 4-2 Contrasting photo-based measurements against tape measurements

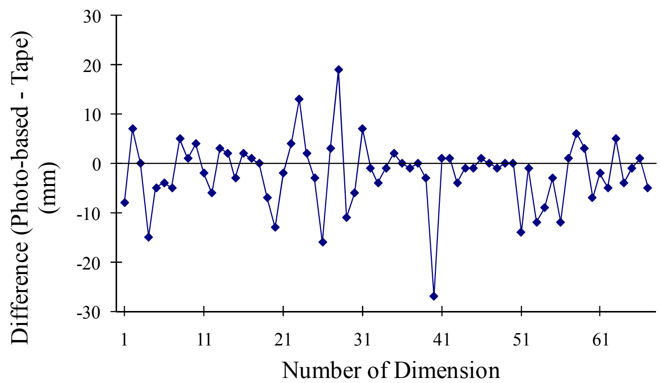

Fig. 4-3 Difference between photo-based measurements and tape measurements

4.4.2 Analytical Assessment of Agreement

Applying regression or correlation coefficient techniques to evaluate the agreement between two sets of measurements taken on the same objects possibly produces biased results (Altman and Bland 1983). To shed light on the biases, we generate two sets of pseudo measurement data, X and Y, as plotted in Fig. 4-4. Both the regression line (slope = 1.02, intercept = 0.83) and the correlation coefficient (r = 0.93) imply the two sets of measurements are well associated; but it can be seen that nearly all the points lie to the left of the line of equality, thus suggesting a lack of agreement between the two sets of data.

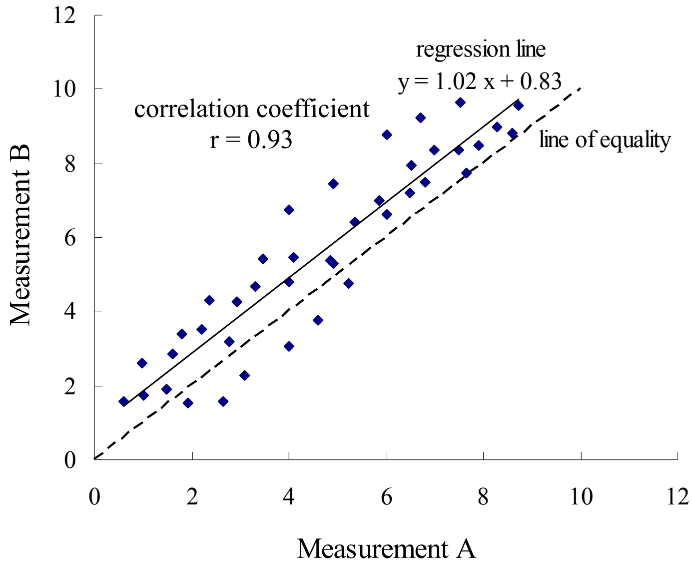

Fig. 4-4 Regression analysis on two sets of pseudo measurement data (dimensionless for illumination)

In addition, the regression and correlation coefficient techniques share one limitation: their results may vary as different data ranges are considered, while the true indicator of agreement should remain stable irrespective of data ranges (Bland and Altman 2003). To illuminate this problem, we segregate the data of the pseudo measurements at an arbitrary cut point of 5. Fig. 4-5 shows that the resulting regression lines and correlation coefficients much depend on the sub-range of measurements. For samples whose values are less than 5, the regression line has a slope of 0.74 and an intercept of

1.36, while the correlation coefficient is 0.73 (Fig. 4-5a); for samples whose values are greater than or equal to 5, the slope is 0.67 and the intercept is 3.42 as of the regression line, while the correlation coefficient is 0.75 (Fig. 4-5b). Note in each case, the value of correlation coefficient (0.75 and 0.73) has considerably decreased compared with the original value of 0.93 derived without dividing the data.

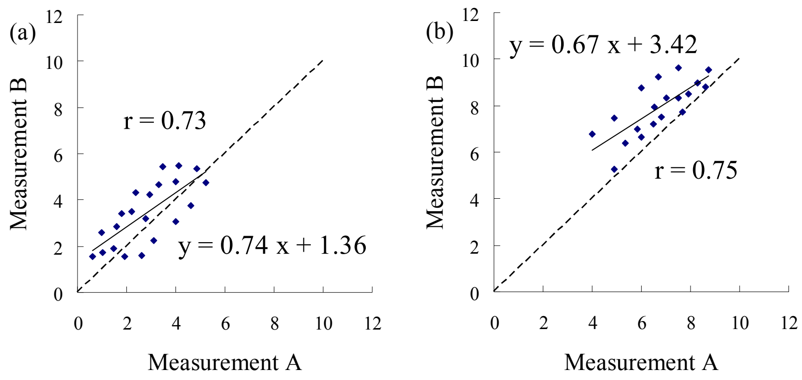

Fig. 4-5 Regression analysis on the two pseudo measurement data at the cut point of 5 (dimensionless for illumination)

4.4.3 95% Limits of Agreement

Applying the "95% limits of agreement" method to assess the agreement of two measurement methods was originally proposed in the medical research (Bland and Altman 1986). This technique has been applied in a wide range of research disciplines (as evidenced by more than 10,000 citations of the original research publication). In the medical discipline, one classical example of applying the 95% limits of agreement was to evaluate the interchangeability of blood pressure measurements between a new type of electronic instrument and the commonplace sphygmomanometer (mercury bars). The new instrument did not pass the test as the 95% limits of agreement for the differences between the two sets of measurements were found to be [-54.7, 22.1] mmHg, far exceeding the generally accepted error of margin in medicine (i.e. within ±10 mmHg) (Bland and Altman 1999). In the present research, we intend to assess the discrepancy between geometric measurements taken on the same building products by photogrammetry and by tape. The nature of our problem is analogous to the blood pressure measurement problem in medicine, lending it well to applying the 95% limits of agreement.

The "95% limits of agreement" method is based on two assumptions on the sample data: (1) the mean and the standard deviation of the differences between the two sets remain constant along the entire range of measurements, and (2) the differences between the two sets roughly follow a normal distribution (Bland and Altman 1995). Fig. 4-6 presents the two plots used to validate the above assumptions for our present problem, namely: (1) the scatter plot of the difference against the average values of the two sets of measurements, and (2) the histogram of the differences. In Fig. 4-6a, all the points scatter around the horizontal axis along the range of measurements, without displaying particular divergence or convergence patterns. This indicates the mean and standard deviation of the differences remain constant. Fig. 4-6b shows that the differences between the two sets appear to follow a normal distribution.

Note as the magnitude of measurement increases, any divergence or convergence trend identified in regard to the differences between the two sets of measurements implies a relationship between the error and the magnitude of measurement. In such cases, to determine the limits of agreement first entails transforming all the measurements by taking logarithm (Bland and Altman 1986) or using a ratio of the differences over the averaged measurements (Linnet and Bruunshuus 1991).

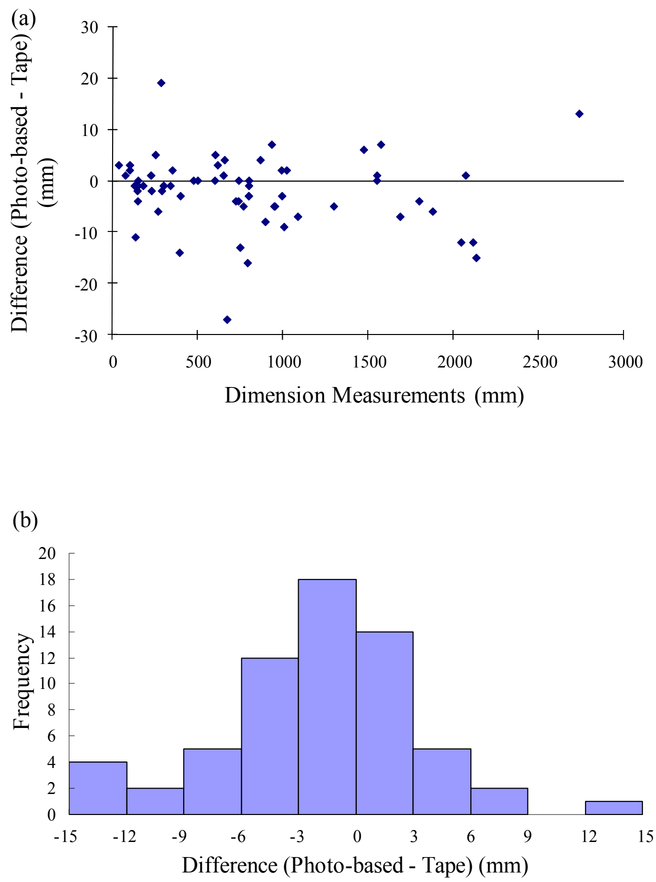

Fig. 4-6 Plots of (a) the scattered measurement difference against the average of photogrammetry and tape measurements and (b) the histogram of the differences

Given the sample mean $\bar{x}$ and the sample standard deviation s of the differences between the two sets of measurements, we have the lower and upper limits of agreement determined by Eq. (4-5):

$$\begin{aligned} Lower\ limit &= \bar{x} - 1.96s \\ Upper\ limit &= \bar{x} + 1.96s \end{aligned} \tag{4-5}$$

Note, 1.96 in Eq. (4-5) is the 95% two-tailed cut value on the standard normal distribution. Then, we would expect with 95% likelihood, the differences between the two sets of measurements fall between the two limits (Bland and Altman 2003). As for our sample data, the mean difference of the photo-based measurement subtracting the tape measurement is -1.96 mm (i.e. $\bar{x}$), and the standard deviation of the difference is 6.81 mm (i.e. s). Hence, by Eq. (4-5), the lower limit and upper limit are determined to be minus 15.30 mm and 11.39 mm respectively. We can state that with 95% likelihood, any geometric measurement of a building product taken by photogrammetry would differ from the corresponding tape measurement by no less than minus 15.30 mm and no more than 11.39 mm.

4.4.4 Confidence Intervals on Limits of Agreement

Analogous to the sample mean and the sample standard deviation, the derived limits of agreement are only estimates based on limited sample data and are subject to change as different samples are taken. To complete the statistical analysis, it is necessary to establish confidence intervals around the estimated values of the limits of agreement so as to infer their true values with respect to the whole population.

First, we establish the 95% confidence intervals for the mean difference between the two sets of measurements by employing the statistic of the *t*-distribution with $n-1$ degrees of freedom. For 95% level of confidence, the interval is represented in Eq. (4-6):

$$[\bar{x} - t_{n-1,0.025} s / \sqrt{n},\ \bar{x} + t_{n-1,0.025} s / \sqrt{n}] \tag{4-6}$$

In the case of our sample data, the sample mean difference $\bar{x}$ is -1.96 mm, the sample size is 67, and $t_{66,0.025}$ is 1.998. The 95% confidence interval for the mean difference is determined as [-3.62 mm, -0.29 mm].

Next, we establish the 95% confidence intervals for the limits of agreement by Eq. (4-7):

$$\begin{aligned} &[LL - t_{n-1,0.025} 1.71 s / \sqrt{n},\ LL + t_{n-1,0.025} 1.71 s / \sqrt{n}] \\ &[UL - t_{n-1,0.025} 1.71 s / \sqrt{n},\ UL + t_{n-1,0.025} 1.71 s / \sqrt{n}] \end{aligned} \tag{4-7}$$

in which *LL* is the lower 95% limit of agreement, *UL* is the upper 95% limit of agreement, and $1.71 s / \sqrt{n}$ is the standard error of the 95% limits of agreement. Note that the mathematical deduction of this standard error is not commonly found in the literature and hence is given in Appendix IV.

In our case, $1.71 s / \sqrt{n}$ equals 1.42 mm. Hence, the 95% confidence interval for the lower limit of agreement is [-15.30 – 1.998 × 1.42] to [-15.30 + 1.998 × 1.42], namely, -18.14 mm ~ 12.46 mm. Similarly, the 95% confidence interval for the upper limit of agreement is [11.39 – 1.998 × 1.42] to [11.39 + 1.998 × 1.42], namely, 8.55 mm ~ 14.23 mm. Fig. 4-7 depicts the 95% confidence intervals for the sample mean difference and the lower and upper limits of agreement in dashed lines.

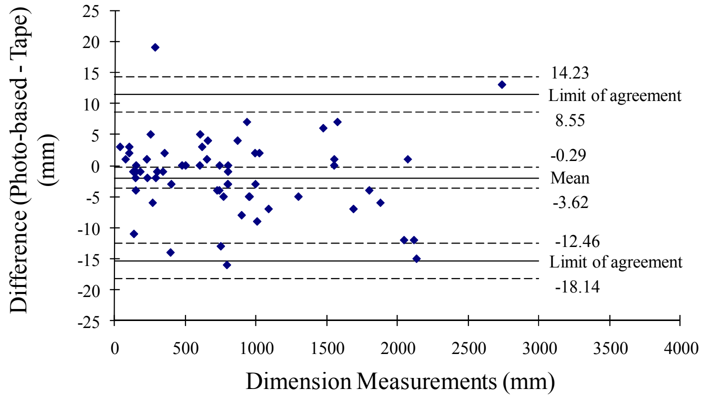

Fig. 4-7 95% confidence intervals for sample mean difference and 95% limits of agreement

The relatively narrow intervals suggest that the 95% limits of agreement derived from the sample data (i.e. [-15.30 mm, 11.39 mm]) can be taken to represent such statistical descriptors for the population. Given particular accuracy requirements in a given construction application, this finding provides the quantitative basis to make decisions on whether to accept or reject photogrammetry as an alternative to conventional tape measurements, as discussed in the next section.

4.5 APPLICABILITY OF PHOTOGRAMMETRY-BASED APPROACH

Photogrammetry provides a potential alternative to the conventional approach to measuring geometric dimensions of building products by tape. Nonetheless, the resulting accuracy of photogrammetry is largely dependent on three factors, namely, (1) the quality of the camera used (such as the optical precision of the lens and the quantity of pixels in forming a digital image), (2) the quality of the photos taken (such as the clarity, the lighting, and the contrast of the picture; the shooting distance between the object and the camera), and (3) the functionality of the photo-processing software applied (e.g., the calibration of a camera, resulting in the determination of the camera's internal parameters for photogrammetry computing).

The photogrammetry-based approach can lend itself well to a particular application setting of construction engineering, such as checking the geometric dimensions of as-built building products or monitoring the settling displacements of control points on an existing building. Nonetheless, it should be ensured that the achievable accuracy level of the photogrammetry-based approach matches up to the desired accuracy level for a particular application before implementing the approach on site. For instance, during the course of the present research, experienced consultant engineers in Hong Kong were interviewed, revealing that the commonly acceptable error tolerance for building settlement monitoring should fall in the order of ±25 mm of the actual vertical dimension measurement. In fact, the photogrammetry-based measurement approach being evaluated throughout the present research has produced the accuracy level sufficient to building settlement monitoring, namely, [-15.30 mm, 11.39 mm] in terms of the 95% limits of agreement as benchmarked against the tape measurements.

In short, the main contribution of the research presented is the formalization of a statistically significant, quantitatively reliable method to assess the accuracy of applying photogrammetry in particular applications of construction engineering. Through weighing the accuracy level achievable by photogrammetry against the accuracy level desirable in a particular application, the engineer makes the final decision on the applicability of the photogrammetry-based approach.

4.6 SUMMARY

The surveying technique of photogrammetry extracts input data from two-dimensional (2D) photo images and maps them onto a three-dimensional (3D) space. In general, photogrammetry provides a potential alternative to the conventional approach to determining geometric dimensions of building products by measurement tape. The photogrammetry-based approach can lend itself well to a particular application setting of construction engineering; examples are checking the geometric dimensions of as-built building products or monitoring the settling displacements of control points on an existing building. By simply taking snapshots of the building product with a digital camera from different angles, a site engineer is able to derive as-built measurements through post processing those photos by use of photogrammetry software.

It is reemphasized that the achievable accuracy level for the photogrammetry-based approach should match up to the desired accuracy level for a particular application prior to implementing the approach on site. The resulting accuracy of photogrammetry is largely dependent on (1) the quality of the camera used, (2) the quality of the photos taken and (3) the functionality of the photo-processing software applied. The main contribution of the research presented is formalizing a statistically significant, quantitatively reliable technique to assess the accuracy of applying photogrammetry for geometric dimension measurements in particular applications of construction engineering. By weighing the accuracy level achievable by the methodology against the accuracy level desirable according to particular application requirements, the engineer makes the final decision on the applicability of the photogrammetry-based approach.

In summary, the very basic technique of photogrammetry is effective and computationally simple. As photogrammetry has been digitized, its application cost has been much reduced while its accuracy keeps improving with technological advances in digital cameras and computer software. The systematic approach we have proposed for assessing the accuracy of photogrammetry is conducive to finding new applications of photogrammetry in construction engineering and management.

CHAPTER 5

AUGMENTING SITE PHOTOS WITH 3D GRAPHICS OF UNDERGROUND INFRASTRUCTURE IN CONSTRUCTION ENGINEERING APPLICATIONS

5.1 INTRODUCTION

This chapter proposes an analytical approach to incorporating computer-generated, three-dimensional (3D) graphics of invisible underground infrastructure into site photos so as to present a richer and more integral view of the site situation in construction engineering applications. The proposed approach simulates the image forming process of a camera and produces a virtual photo of the underground scene, whose virtual coordinate axes coincide with the real coordinate axes of the aboveground site scene. As a result, the virtual photo and the site photo can be seamlessly merged in terms of perspective, position, and scale. This research simplifies the calculation of the camera's spatial orientation by use of the coordinates of only two reference points, namely, the camera station position and the object focus position. The whole procedure of the proposed approach is analytical and can be automated into a computer program. In practice, non-destructive subsurface imaging technologies are commonly used to obtain the profile data of the as-built underground infrastructure, which can be readily processed into a 3D as-built model as one component in composing the virtual underground scene. The proposed approach is demonstrated with two case studies in which (1) the underground as-built data is superimposed into the site photo for the purpose of quality investigation of a bored pile construction and (2) the micro-tunneling site photo is augmented with the as-built concrete sleep pipe at particular time events to visualize the dynamic progress of construction.

5.2 OVERVIEW OF ANALYTICAL PHOTO-AUGMENTING METHOD

Fig. 5-1 presents a schematic overview of the proposed method, illustrating the concept of augmenting 3D models of underground infrastructure onto a site photo. When photographing a construction jobsite with a camera, only a surface object that falls on the line of sight of a camera lens can be captured in the photo image. However, depiction of the jobsite situation usually requires inclusion of subsurface building products as well. For instance, as shown on the left side of Fig. 5-1, at a foundation jobsite a bore hole has been excavated in the ground for constructing a pile and it is desirable to visualize the underground construction progress in the site photo. To compensate for the loss of subsurface information due to invisibility, a virtual camera is set up to photograph the excavation hole in a virtual 3D modeling environment as shown in the right side of Fig. 5-1. The basic idea of this approach is to place a camera in the same position and orientation as on the actual jobsite and simulate the image forming process of a camera in the virtual environment. The virtual photo of the site scene coincides exactly with the real site photo in terms of perspective, position, and scale. As a result, the virtual photo is readily overlaid over the real jobsite photo to show the "invisible" information of the underground infrastructure.

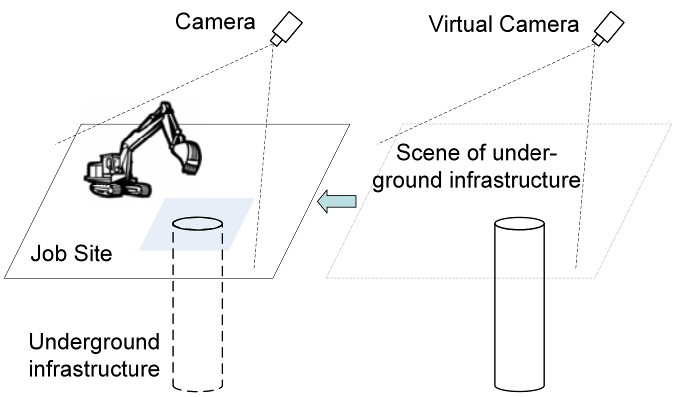

Fig. 5-1 Overview of proposed methodology for immersing invisible underground infrastructure into site photo

To augment photos with virtual 3D models generally requires the determination of the camera's position (i.e. the position coordinates) and orientation (as described by three rotation angles). To make it practical for construction applications, the analytical photo-augmenting method proposed simplifies input data requirements and only entails the determination of two reference points' positions in the site coordinate system, namely, the camera station position and the object focus position. The photo-augmenting equations are derived to calculate the three rotation angles based on the coordinates of the two reference points, eliminating the need of using an orientation measurement device (e.g., compass or gyroscope). This results in simplified analytics and practical procedures of site data collection. With the position and orientation of the camera known, given any point of a 3D model, the photo-augmenting equations are essentially applied to calculate the exact coordinates in the 2D grid of a photo image. As a result, the virtual 3D model is merged into the site photo without any manual matching operations such as cropping, rotating, and scaling. The entire photo-augmentation procedure is analytical and can be automated into a computer program.

Data of as-built underground infrastructure can be acquired by subsurface imaging technologies, which is provided as the input to generating the 3D as-built model. With the proposed approach, the 3D underground infrastructure model can be analytically and accurately *computed* into a 2D photo of the site scene. The following section will elaborate on deduction of the photo-augmenting equations in detail.

5.3 PHOTO-AUGMENTING EQUATIONS

The photo-augmenting equations are based on the imaging mechanism formalized in the optical science. The imaging mechanism is concerned with the process that the reality in the 3D space is projected onto the flat film of the camera, generating a view of a 3D scene at a particular time. The core of this process is to establish the linkage between the position of a point in the three dimensional space and the position of the same point on the camera image plane (film). The following section introduces the camera imaging mechanism, based on which, the mathematical equations are formulated to allow for parameterization of projecting a 3D model onto a 2D photo image.

5.3.1 Camera Imaging Mechanism

To take a photo, we need first to position the camera at a particular location in the space. Next is to setup the camera's orientation: At which direction we point the camera and how we rotate it to fix its perspective. Finally, we frame a scene tailored to the size of the aperture of the camera. By snapping the shutter, light reflected from the visible surface in the scene is projected through the camera's lens onto the image plane of the camera. Fig. 5-2 gives an illustration of a camera's position and orientation when photographing an object. Next, the mathematical relationship will be established between the positions of a point in the object space and in the image plane of the camera.

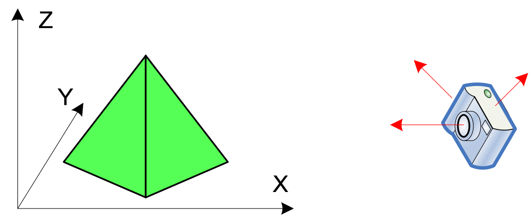

Fig. 5-2 A camera's position and orientation when photographing a scene

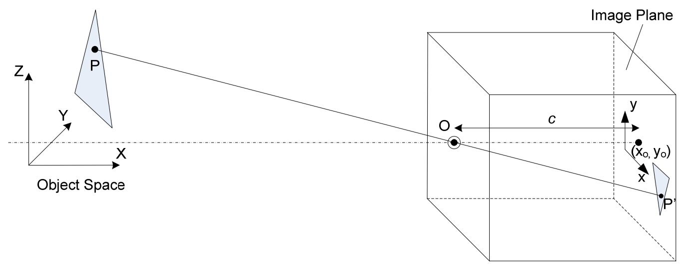

Fig. 5-3 Camera image forming mechanism

The coordinate system in the object space is defined as the object coordinate system, and the one in the image plane is defined as the image coordinate system. Both coordinate systems are right-handed Cartesian. Fig. 5-3 shows the camera's image forming mechanism. The lens of the camera is modeled by a needle hole *O*, known as the perspective center and its location in the object space is (X_o, Y_o, Z_o). The *principal distance* (*c* in Fig. 5-3) refers to the distance of the perpendicular line from the perspective center *O* to the image plane; the *principal point* (x_o, y_o in Fig. 5-3) is where the line intersects the image plane. Note the *principal distance c* can be approximated as the camera's *focal length f*.

The orientation of the camera is characterized by three Euler rotation angles. Ideally, the object point (*P*), the perspective center (*O*), and the image point (*P'*) are aligned along a straight line as shown in Fig. 5-3. This yields the *collinearity* condition in which the vector *OP'* aligns with the vector *OP*, formulated as:

$$\begin{bmatrix} x_n - x_o \\ y_n - y_o \\ -c \end{bmatrix} = \lambda \boldsymbol{M} \begin{bmatrix} X_n - X_o \\ Y_n - Y_o \\ Z_n - Z_o \end{bmatrix}. \tag{5-1}$$

In Eq. (5-1), $\boldsymbol{M}$ is the 3×3 rotation matrix, λ is the scale factor, and $\boldsymbol{p_n} = (x_n, y_n)^T$ and $\boldsymbol{P_n} = (X_n, Y_n, Z_n)^T$ are the coordinates of the *n*th point in the image plane and the object space, respectively. Assume that m_{ij} $(i, j = 1, 2, 3)$ are the elements of the rotation matrix $\boldsymbol{M}$, algebraic manipulation of Eq. (5-1) yields the *Collinearity Equations* (as Eq. 5-2), which relates the position of the *n*th point in the object space to the position of its image point in the image plane (Wong 1980; Wolf 1983; McGlone 1989):

$$\begin{aligned} x_n &= x_o - c\frac{m_{11}(X_n - X_o) + m_{12}(Y_n - Y_o) + m_{13}(Z_n - Z_o)}{m_{31}(X_n - X_o) + m_{32}(Y_n - Y_o) + m_{33}(Z_n - Z_o)}, \\ y_n &= y_o - c\frac{m_{21}(X_n - X_o) + m_{22}(Y_n - Y_o) + m_{23}(Z_n - Z_o)}{m_{31}(X_n - X_o) + m_{32}(Y_n - Y_o) + m_{33}(Z_n - Z_o)}. \end{aligned} \tag{5-2}$$

By Eq. (5-2), X, Y, Z coordinates of the object point in the object space can be analytically transformed into x, y coordinates of the corresponding image point in the image plane.

5.3.2 Rotation Matrix Determination

In this section, the rotation angles azimuth (α), tilt (t), and swing (s) are defined for determining the rotation matrix $\boldsymbol{M}$ (Wolf 1983), by which the orientation of the camera in the object space are fixed. Fig. 5-4 shows the three rotation angles in relation to the camera image plane. In Fig. 5-4, the point O is the perspective center of the camera, and o is the principal point on the image plane. Projecting O onto the XY-plane of the object coordinate system yields the point P_o, Oo is perpendicular to the image plane, and the extension of the line Oo intersects the XY-plane yielding the point P_d. By plotting an auxiliary Y'-axis passing through P_o on the XY-plane, azimuth (α) is defined as the clockwise angle measured from the Y'-axis to the line P_oP_d. Tilt (t) is the angle between the vertical line OP_o and the camera optical axis OP_d. The vertical line OP_o intersecting the image plane yields the point n. n is the *photographic nadir point*. Swing (s) is defined as the clockwise angle measured on the image plane from the positive vertical axis y to the vector *on* (from the principal point to the nadir point). Actually, the line *on* is where the vertical plane which is parallel to YZ-plane intersects with the image plane.

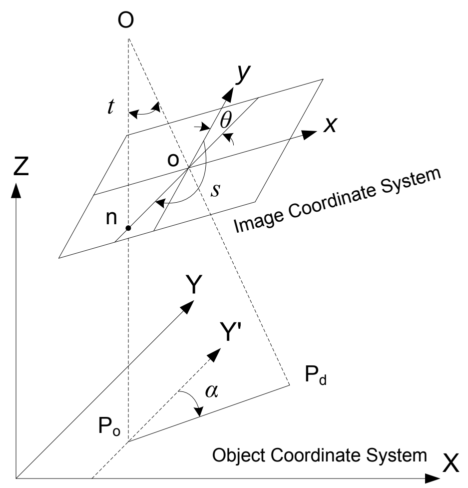

Fig. 5-4 The camera image plane showing the three angular orientations - azimuth, tilt, and swing

To simplify the explanation, the rotation matrix determination is demonstrated first with the rotation in two-dimensional plane. Assume that an xy-coordinate system is rotated from the XY-coordinate system with an angle α and the point P's coordinates in the xy-coordinate system are x and y, the coordinates X and Y of P in the XY-coordinate system can be calculated (Fig. 5-5). In Fig. 5-5, the xy-coordinate system results from rotating the XY-coordinate system clockwise by α; and the coordinates X and Y of the point P can be determined as:

$$\begin{aligned} X &= x\cos\alpha + y\sin\alpha, \\ Y &= -x\sin\alpha + y\cos\alpha. \end{aligned} \tag{5-3a}$$

Representing Eq. (5-3a) with vector and matrix yields:

$$\boldsymbol{X} = \begin{pmatrix} X \\ Y \end{pmatrix} = \begin{pmatrix} \cos\alpha & \sin\alpha \\ -\sin\alpha & \cos\alpha \end{pmatrix} \begin{pmatrix} x \\ y \end{pmatrix} = \boldsymbol{Rx}. \tag{5-3b}$$

Note, if the rotation direction is counter-clockwise, the angle α should be set negative in Eq. (5-3b) in calculating the coordinates X, Y.

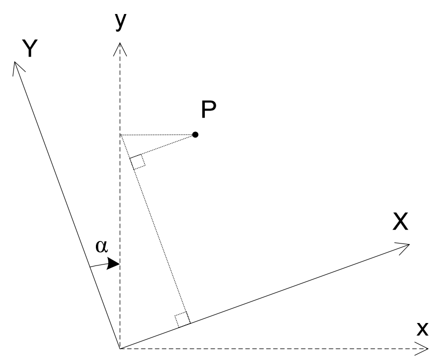

Fig. 5-5 Coordinate system rotation in the two-dimensional plane

For the rotation matrix M, the elements m_{ij} are functions of three rotation angles *(α, t, s)*. By use of *α, t, s*, the object coordinate system can be analytically rotated to be aligned with the image coordinate system. To develop the rotation formulas, the object coordinate system and the image coordinate system are both translated with the origins set to the camera perspective center O, denoted by the XYZ-coordinate system and the xyz-coordinate system respectively (Fig. 5-6a). As shown in Fig. 5-6, the XYZ-coordinate system rotates into the xyz-coordinate system in three sequential steps. Each step rotates about one axis and accordingly changes the positions of the other two axes (Fig. 5-6b-d). Now, in independent steps, we repeat the rotation from the XYZ-coordinate system to the xyz-coordinate system in order to determine the rotation matrix.

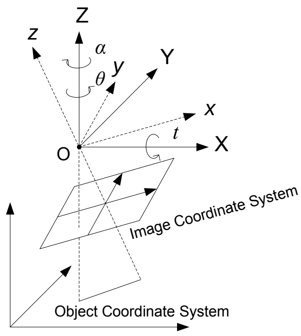

(a) Rations in azimuth, tilt, and swing

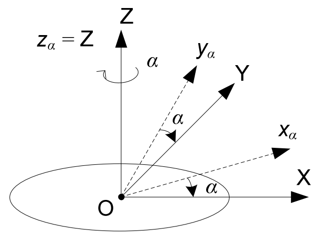

(b) First rotation in azimuth

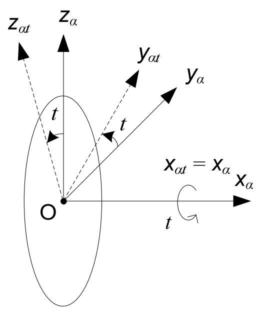

(c) Second rotation in tilt

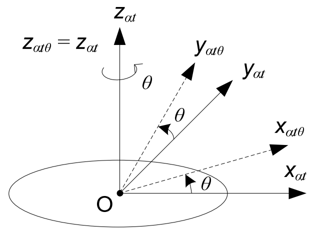

(d) Third rotation in swing

Fig. 5-6 Rotations of azimuth, tilt, and swing in the three-dimensional space

Step 1 is to rotate by azimuth (α), in which the XYZ-coordinate system rotates a clockwise angle α about the Z-axis to generate an $x_\alpha y_\alpha z_\alpha$-coordinate system (Fig. 5-6b). The coordinates of any point in the XYZ-system can be calculated from the $x_\alpha y_\alpha z_\alpha$-system by:

$$\boldsymbol{X} = \begin{pmatrix} \cos\alpha & \sin\alpha & 0 \\ -\sin\alpha & \cos\alpha & 0 \\ 0 & 0 & 1 \end{pmatrix} \begin{pmatrix} x_\alpha \\ y_\alpha \\ z_\alpha \end{pmatrix} = \boldsymbol{R_\alpha x_\alpha}. \tag{5-4}$$

Step 2 is to rotate by tilt (t), in which the $x_\alpha y_\alpha z_\alpha$-coordinate system rotates a counter-clockwise angle about the x_α-axis to generate an $x_{\alpha t} y_{\alpha t} z_{\alpha t}$-coordinate system

(Fig. 5-6c). Since the rotation is counter-clockwise, we add a minus sign (-) before the angle to evaluate the rotation matrix. The coordinates of any point in the $x_\alpha y_\alpha z_\alpha$-system are derived from the $x_{\alpha t} y_{\alpha t} z_{\alpha t}$-system as:

$$\boldsymbol{x_\alpha} = \begin{pmatrix} 1 & 0 & 0 \\ 0 & \cos t & -\sin t \\ 0 & \sin t & \cos t \end{pmatrix} \begin{pmatrix} x_{\alpha t} \\ y_{\alpha t} \\ z_{\alpha t} \end{pmatrix} = \boldsymbol{R_t x_{\alpha t}}. \tag{5-5}$$

In Step 3, the third rotation of swing is performed with regard to the angle θ, which is defined by $\theta = s - 180^o$ (Fig. 5-4). The rotation of the angle θ is counter-clockwise about the $x_{\alpha t}$-axis, resulting in the $x_{\alpha t\theta} y_{\alpha t\theta} z_{\alpha t\theta}$-coordinate system which coincides with the xyz-system (Fig. 5-6d). The coordinates of any point in the $x_{\alpha t} y_{\alpha t} z_{\alpha t}$-system from the $x_{\alpha t\theta} y_{\alpha t\theta} z_{\alpha t\theta}$-system can be calculated by:

$$\boldsymbol{x_{\alpha t}} = \begin{pmatrix} \cos\theta & -\sin\theta & 0 \\ \sin\theta & \cos\theta & 0 \\ 0 & 0 & 1 \end{pmatrix} \begin{pmatrix} x_{\alpha t\theta} \\ y_{\alpha t\theta} \\ z_{\alpha t\theta} \end{pmatrix} = \boldsymbol{R_\theta x}. \tag{5-6a}$$

Substituting $\theta = s - 180^o$ into Eq. (5-6a), we have:

$$\boldsymbol{x_{\alpha t}} = \begin{pmatrix} -\cos s & \sin s & 0 \\ -\sin s & -\cos s & 0 \\ 0 & 0 & 1 \end{pmatrix} \begin{pmatrix} x_{\alpha t s} \\ y_{\alpha t s} \\ z_{\alpha t s} \end{pmatrix} = \boldsymbol{R_s x}. \tag{5-6b}$$

Now, we back substitute Eq. (5-6b) into Eq. (5-5) and Eq. (5-4) in turn, yielding: $\boldsymbol{X} = \boldsymbol{R_\alpha R_t R_s x} = \boldsymbol{Rx}$. Because the rotation matrix $\boldsymbol{M}$ is about the mapping of coordinates from the XYZ-system to the xyz-system, we transform $\boldsymbol{X} = \boldsymbol{Rx}$ into $\boldsymbol{x} = \boldsymbol{R^{-1}X}$, where

$\boldsymbol{R^{-1}}$ is the inverse matrix of $\boldsymbol{R}$. $\boldsymbol{R}$ is orthogonal, thus $\boldsymbol{R^{-1}}$ equals the transposed matrix $\boldsymbol{R^T}$. By calculation, $\boldsymbol{R^T}$ can be represented as:

$$\boldsymbol{M} = \boldsymbol{R}^T = \begin{bmatrix} m_{11} & m_{12} & m_{13} \\ m_{21} & m_{22} & m_{23} \\ m_{31} & m_{32} & m_{33} \end{bmatrix}, \tag{5-7a}$$

where

$$\begin{aligned}
m_{11} &= -\cos\alpha\cos s - \sin\alpha\cos t\sin s, \\
m_{12} &= \sin\alpha\cos s - \cos\alpha\cos t\sin s, \\
m_{13} &= -\sin t\sin s, \\
m_{21} &= \cos\alpha\sin s - \sin\alpha\cos t\cos s, \\
m_{22} &= -\sin\alpha\sin s - \cos\alpha\cos t\cos s, \\
m_{23} &= -\sin t\cos s, \\
m_{31} &= -\sin\alpha\sin t, \\
m_{32} &= -\cos\alpha\sin t, \\
m_{33} &= \cos t.
\end{aligned} \tag{5-7b}$$

5.3.3 Camera Orientation Determination

In practice, it is not straightforward to directly measure the three rotation angles of a camera station by use of gyroscope or compass when taking a picture on a construction site. To set out the actual positions of building products, points with known coordinates (referred to as *reference points*) are predefined in the site. As far as the operational feasibility is concerned, the coordinates of the camera location and reference points in the site are much easier to obtain by use of commonplace surveying instruments (such as total station or GPS). According to Eq. (5-2), at least three known points are required to solve for the total six parameters of the rotation matrix. However, determination of the values of those parameters involves non-linear, iterative calculation which may lead to solution divergence (Dewitt 1996). To overcome this hurdle, the direct linear transformation (DLT) method, originally proposed by Abdel-Aziz and Karara (1971), is applied to simplify the *Collinearity Equations* into a linear form by re-arranging and combining terms in Eq. (5-2), as given in Eq. (5-8). Note the eleven DLT parameters ($L_1, \ldots, L_{11}$) are functions of the camera parameters $(X_o, Y_o, Z_o, \alpha, t, s, c, x_o, y_o)$.

$$
\begin{aligned}
&L_1 X_n + L_2 Y_n + L_3 Z_n + L_4 - x_n (L_9 X_n + L_{10} Y_n + L_{11} Z_n + 1) = 0, \\
&L_5 X_n + L_6 Y_n + L_7 Z_n + L_8 - y_n (L_9 X_n + L_{10} Y_n + L_{11} Z_n + 1) = 0.
\end{aligned}
\tag{5-8}
$$

It is noteworthy that derivation of the simple equation form incidentally adds to the number of the initial DLT parameters, thus requiring at least six known points in solving the equations (Eq. 5-8).

5.3.4 Two-Point Method to Fix Camera Orientation

The present research is intended to devise a pragmatic method by which the camera station's orientation can be determined with the minimal input data, namely, the camera station position and the object focus position. The camera station position is the coordinates of the camera perspective center and the object focus position is the focused point of the framed photo that is referred to as the point on the surface of the object at which the camera is aimed through the center focus point in the viewfinder of the camera when taking pictures in the auto-focus (AF) mode. Note if a camera provides multiple focus points on the camera' viewfinder, the autofocus function needs to be set the focus point to the center point of the viewfinder. Fig. 5-7 shows the camera station position and the object focus position in the object coordinate system, which are denoted as P_o (X_o, Y_o, Z_o) and P_f (X_f, Y_f, Z_f) respectively. Because the x, y axes of the image coordinate system lie on the image plane of the camera, connecting P_o and P_f forms a line along the z-axis and is perpendicular to the image plane of the camera. Hence, we can specify a vector to represent this line, that is:

$$\boldsymbol{N} = \begin{bmatrix} X_f - X_o \\ Y_f - Y_o \\ Z_f - Z_o \end{bmatrix}. \tag{5-9}$$

$\boldsymbol{N}$ aligns along the z-axis of the image coordinate system. Actually, it is the normal vector of the camera image plane which can be expressed in terms of rotation angles α and t.

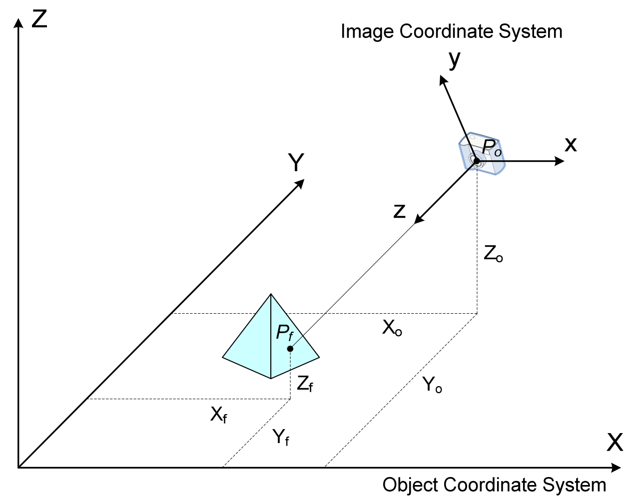

Fig. 5-7 The camera station position and the object focus position in the object coordinate system

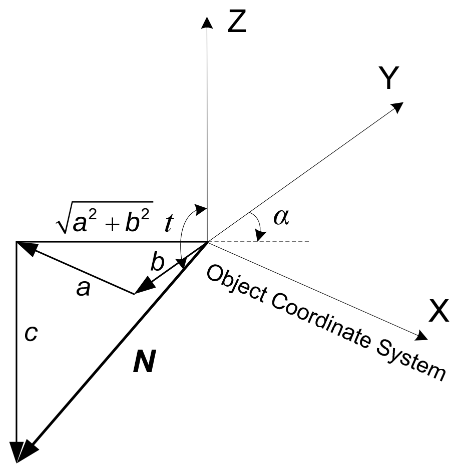

Fig. 5-8 The normal vector *N* at origin of the object coordinate system

Now we use ***N*** to derive the camera's rotation angles *(α, t)*. The ranges of values of three rotation angles are set as:

$$\alpha \in (-180^o, 180^o],$$
$$t \in [0^o, 180^o],$$
$$s \in (-180^o, 180^o].$$

This ensures each possible angle combination uniquely describes the spatial relationship between the two sets of coordinate systems, thus avoiding the duality problem in solving triangular equations (Shih 1990). To determine *α* and *t*, Fig. 5-8 is plotted to illustrate the normal vector ***N*** at the origin of the object coordinate system, where symbols of *a, b,* and *c* are defined as:

$$\begin{aligned} a &= X_f - X_o, \\ b &= Y_f - Y_o, \\ c &= Z_f - Z_o. \end{aligned} \tag{5-10}$$

In Fig. 5-8, t is determined by calculating the elevation angle of $\boldsymbol{N}$ with respect to the XY-plane, as per:

$$t = 90^o - \arctan(\frac{c}{\sqrt{a^2 + b^2}}). \tag{5-11}$$

α is determined by projecting $\boldsymbol{N}$ onto the XY-plane and calculating the angle of the projection with respect to the Y-axis, as per:

$$\alpha = \arctan(\frac{a}{b}). \tag{5-12}$$

As for Eq. (5-12), attention should be given to the proper quadrant selection of the angle, as described by the sign of the numerator -a and denominator -b, which requires the use of the full-circle inverse tangent function (e.g., atan2 in C or FORTRAN) to calculate the complete range of the desired angle (-180^o ~ 180^o).

It is worth mentioning that to compute the third rotation angle s only based on the normal vector N is not sufficient. Herein, it is reasonably assumed site photos are taken in either "landscape" or "portrait" mode, which means the camera is always held in such a way that one of the x and y axes in the image coordinate system parallels the surface formed by X and Y axes in the object coordinate system. As such, the rotation angle s of the camera is equal to 180^o (landscape position) or -90^o (counter-clockwise portrait position), or 90^o (clockwise portrait position) (shown in Fig. 5-9). It is noted that when applying this method in construction applications, such an imposed requirement of camera's rotation is practically acceptable. This results in the minimal effort involved in preparing input data for calibrating the camera's position and orientation at a real construction site.

(a) 180° (landscape position)

(b) -90° (counter-clockwise portrait position)

(c) 90° (clockwise portrait position)

Fig. 5-9 The photographing condition about the swing rotation of the camera

5.3.5 Calculation Example

To verify the above equations and illustrate their application, we simply locate the camera station position (P_o) and the object focus position (P_f) along the X-axis; P_o $(10, 0, 0)$ and P_f $(0, 0, 0)$ are shown in Fig. 5-10. The camera is positioned in the landscape mode (s = 180°) with the focal length f set as 14 mm. By quick trigonometric calculation, projecting an object point P_n $(0, 4, 3)$ onto the image plane of the camera yields the point's coordinates p_n $(5.6, -4.2)$ in the image plane: x = 4 × 14 / 10 = 5.6 mm, y = - 3 × 14 /10 = -4.2 mm. Alternatively, we compute the point's coordinates in the image plane by the proposed equations Eq. (5-11) and (5-12), yielding α = 90°, t = 90°, s = 180°. Thus, the rotation matrix Eq. (5-7b) is determined as:

$$\boldsymbol{M} = \begin{bmatrix} 0 & -1 & 0 \\ 0 & 0 & 1 \\ -1 & 0 & 0 \end{bmatrix}. \qquad \text{(5-13a)}$$

By Eq. (5-2), we have the collinearity equations:

$$\begin{aligned} x_n &= \frac{14Y_n}{-X_n + 10}, \\ y_n &= \frac{-14Z_n}{-X_n + 10}. \end{aligned} \qquad \text{(5-13b)}$$

By Eq. (5-13b), the same image coordinates p_n *(5.6, -4.2)* are obtained.

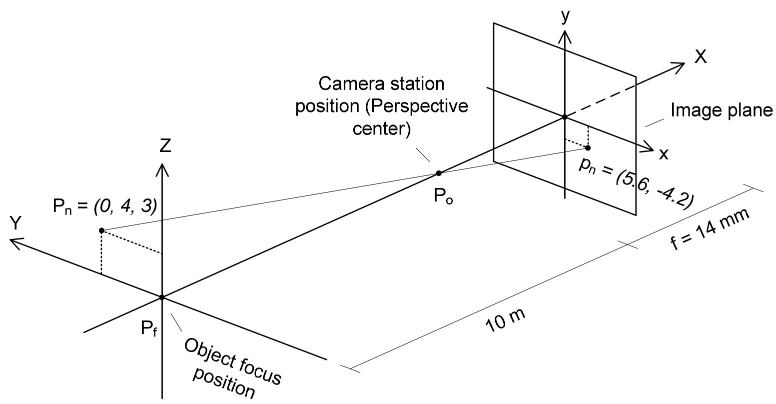

Fig. 5-10 Perspective projection of an object point P_n with coordinates *(0, 4, 3)* to the position p_n *(5.6, -4.2)* on the image plane (the focal length exaggerated for clarity)

In the following section, the proposed analytical approach is applied in two practical cases of construction engineering applications to further demonstrate its usefulness.

5.4 APPLICATION CASE: BORED PILE EXCAVATION

Construction of underground infrastructure such as bored piles features invisibility of subsurface workspace and uncertainty of geotechnical conditions. This has largely accounted for the difficulty and challenge being experienced by site investigators in checking the quality of the built underground infrastructure and monitoring construction progress. Emerging non-destructive subsurface imaging technologies (e.g., ultrasonic waves, ground penetrating radars) have been employed in practice for delineating the features of the underground infrastructure. Ultrasonic or radio waves are applied to acquire information of actual distributions of physical and geometrical properties in order to describe as-built conditions and indicate the position of the underground infrastructure (Jeong and Abraham 2004). To acquire the as-built geometric data of invisible underground infrastructure, subsurface imaging technologies are generally employed in construction, such as electromagnetic methods, magnetic methods and acoustic emission methods (Jeong and Abraham 2004). In this section, the Koden test is briefly introduced, which is the common practice for quality inspection of bored pile excavation in Hong Kong building sites.

5.4.1 Ultrasonic Profiling of Pile Excavation

Koden test makes use of ultrasonic waves to detect the internal walls of a bore hole and measure the dimensions of the excavated shaft. The test instruments consist of a four-direction ultrasonic wave sensor, a winch system to lower and lift the sensor inside the bore hole, and a data logging controller to record and export measurement data. The four-direction ultrasonic sensor takes measurements in two orthogonal directions defined as XX′-axis and YY′-axis respectively (Fig. 5-11a). As the sensor is lowered or lifted inside the bore hole, ultrasonic waves are emitted and propagated through the filling fluid (water or bentonite). As the ultrasonic wave reaches the wall surface, it is bounced back and received by the sensor. By measuring the duration of ultrasonic wave propagation, the geometric profile of bore hole sidewalls can be obtained. The recorded data contain the verticality of sidewalls, the diameter of the hole, dimensions of the bellout (pile foot) and the depth of excavation (Fig. 5-11b). A three-dimensional, as-built model of the bored pile can be quickly built based on the Koden test results.

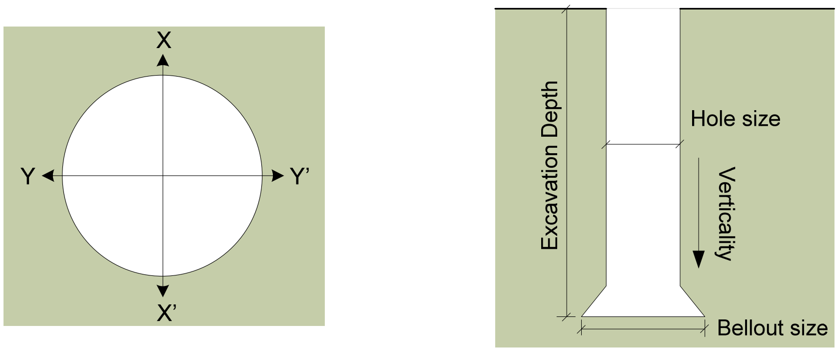

(a) Plan view of the bored pile (b) Elevation view of the bored pile

Fig. 5-11 Orthographic projection views of the bored pile

To demonstrate the practical feasibility of this analytical approach, the Koden test data resulting from a bored pile excavation at a building site in Hong Kong was used to produce the 3D as-built model, followed by immersing this 3D as-built bored pile model into the site photo by computation.

Fig. 5-12 shows the Koden test instrument (a Koden Ultrasonic Drilling Monitor Model DM-602/604) and the raw format of the test result. In Fig. 5-12b, both the profiles of the bore hole along XX′-axis and YY′-axis are plotted. The raw images were transformed into the computer-aided design (CAD) drawing annotated with geometric parameters (Fig. 5-13). Note that out-of-tolerance inclination was identified below Level L: the inclination ratio was measured as 1/58, exceeding the threshold value 1/300 as per technical specifications.

(a) Koden Ultrasonic Drilling Monitor DM-602/604

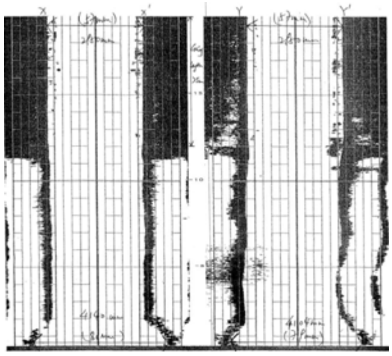

(b) Test result from Koden DM-602/604

Fig. 5-12 Koden Ultrasonic Drilling Monitor DM-602/604 and the test result

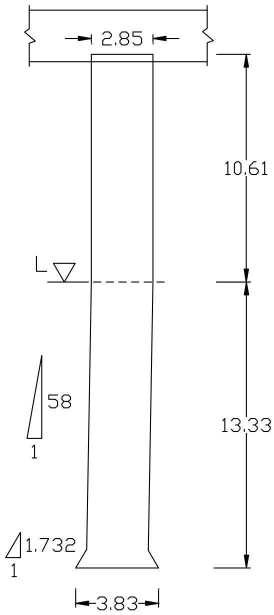

Fig. 5-13 The computer-aided design drawing of the bored pile annotated with geometric parameters

5.4.2 Virtual Photography

In this case, we simulated the photo-taking process by setting up a virtual camera in the virtual environment as follows: we applied 3ds Max® (Autodesk 2009) to quickly model the 3D as-built bored pile. We then set up a virtual camera in the 3ds Max® environment with the camera settings as: s = 180° (landscape mode); camera station position P_o *(-18, -7.5, 5)*. Note that the object coordinate system has its origin at the top center of the bored pile and the unit of coordinates is meter. The object focus position of the photo P_f *(-1.425, 0, 0)* was set at the edge of the cross section of the bored pile's top (Fig. 5-14).

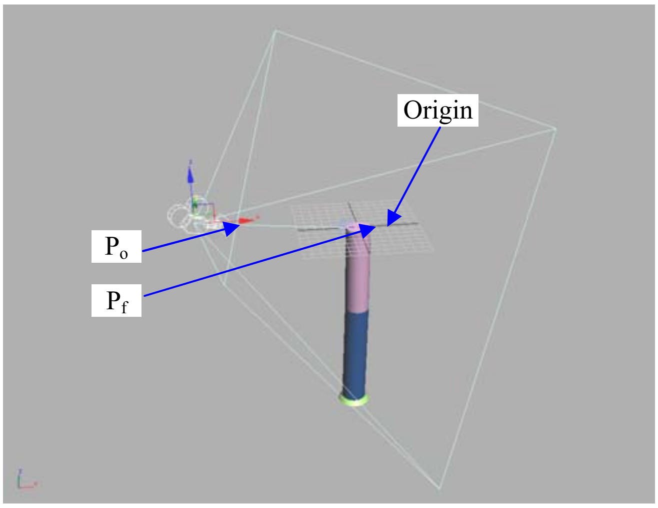

Fig. 5-14 The virtual camera photographing the 3D as-built model of the bored pile in 3ds Max® environment

Since we have (a = 16.575, b = 7.5, c = -5), by Eq. (5-11) and (5-12), we calculated the other two rotation angles of the virtual camera as:

$$\alpha = \arctan(\frac{16.575}{7.5}) = \arctan 2(\frac{-16.575}{-7.5}) = -114.35^o. \tag{5-14}$$

$$t = 90^o - \arctan(\frac{-5}{\sqrt{16.575^2 + 7.5^2}}) = 105.37^o. \tag{5-15}$$

With the three rotation angles known, we have the rotation matrix determined by Eq. (5-6b):

$$\boldsymbol{M} = \begin{bmatrix} -0.412249 & 0.911071 & 0.000000 \\ 0.241440 & 0.109249 & 0.964247 \\ 0.878497 & 0.397510 & -0.265007 \end{bmatrix}. \tag{5-16}$$

Further substituting the values of elements m_{ij} and the camera's focal length (14 mm) into Eq. (5-2), the coordinates of any point on the image plane can be determined from the following equations (dimension units in mm):

$$\begin{aligned} x_n &= \frac{5.77149X_n - 12.755Y_n + 8.22437}{0.878497X_n + 0.397510Y_n - 0.265007Z_n + 20.1193}, \\ y_n &= \frac{-3.38016X_n - 1.52948Y_n - 13.4995Z_n - 4.81672}{0.878497X_n + 0.397510Y_n - 0.265007Z_n + 20.1193}. \end{aligned} \tag{5-17}$$

For validation, if P_f *(-1.425, 0, 0)* is entered into Eq. (5-17), the image coordinates are determined as *(0, 0)*, which means the point which lies on the line of sight of the camera is projected onto the center of the image plane. Hence, the whole range of the 3D as-built pile excavation model can be mapped on the site photo analytically. Fig. 5-15 illustrates the augmented site photo of the as-built bored pile excavation. Note the section below Level L with out-of-tolerance inclination is highlighted in blue.

Fig. 5-15 The augmented site photo showing both aboveground and underground information of the bored pile

5.5 APPLICATION CASE: MICRO-TUNNELING

A second case of applying the proposed approach was to augment a micro-tunnel of concrete sleeve pipe into the site photo for the purpose of monitoring the installation of pipe across the So Kwun Wat Nullah in Hong Kong. In order to verify the applicability of the proposed research by practitioners, a senior civil engineering student at Hong Kong Polytechnic University (Ming Fung Siu) was instructed to apply the developed method to conduct the case study independently during May to June 2009.

The construction was to apply micro-tunneling and pipe jacking to install a utility tunnel with an internal diameter of 1.2 m (Fig. 5-16a). Two parallel micro-tunnels were planned to be constructed. During the time the case was conducted, the construction of the micro-tunnel for electrical cable had been completed and the other was in the planning stage (Fig. 5-16b).

(a) (b)

Fig. 5-16 Snapshots of (a) the concrete sleeve pipe and (b) the jacking pit

5.5.1 Site Constraints

Site investigation was carried out in order to determine the possible locations for setting up the camera station and fixing the object focus position in the context of site constraints.

To identify a camera location that covers a complete view of the construction site was difficult. The two jacking pits located at different places with a nullah in between. The camera location should be carefully selected to provide a clear view to show features on the surface and to cover the underground tunnel being built. The main site constraints in this case were the vegetation obstructing the view when taking photos, inaccessible locations within the confines of private residences as well as too high or too far locations to capture site photos in sufficient details.

The object focus position was not selected at the centre of the nullah because the location coordinates on the surface of nullah could not be accurately determined. Instead, the object focus position was determined near the centre of the construction site with its coordinates readily available.

5.5.2 On-Site Photography and Surveying

After the locations of the camera station and the object focus had been determined, the photo captured for augmentation was shown in Fig. 5-17. The camera used was the Canon SLR EOS 400D. In the construction site, there were known surveyed control points used to define the location coordinates (Easting, Northing and Zenith), which were used to link the local coordinates system with the world geodetic system. The total station, reflector and measuring tape were applied in determining the coordinates of the camera's location. The camera station position and the object focus position surveyed were (817537.3, 825641.0, 10.85) and (817574.5, 825675.1, 3.10) respectively (unit: m). The micro-tunnel as-built data were collected once a week by the contractor using a total station and prisms. Each time, a worker entered into the tunnel to place the prism at particular chainages for the total station to survey the pipe invert position and the alignment deviations of the as-built tunnel against as-designed. We acquired the data from the contractor and used them together with the design data of the concrete sleeve pipe to build the 3D as-built tunneling model in 3ds Max®.

Fig. 5-17 The photo used for augmentation

5.5.3 Photo Augmentation

In 3ds Max®, the 3D models of the jacking pit and the concrete sleeve pipe were built based on the data from the shop drawings. All the coordinates were transformed from the world geodetic system to a local coordinate system. The local system was set as: the origin was at the centre of the cross section at the starting end of the micro-tunnel hosting the electrical cable; the coordinates of the camera's perspective position P_o and the object focus position P_f were (26.640, 238.713, 15.003) and (2.560, 194.200, 7.250) (unit in meter). With the values of the normal vector N determined (a = -24.08, b = -44.513, c = -7.753), we calculated three orientation angles as ($\alpha = 28.41^o$, $t = 98.71^o$, $s = 180^o$).

$$\alpha = \arctan(\frac{-24.080}{-44.513}) = \arctan 2(\frac{24.080}{44.513}) = 28.41^o \tag{5-18}$$

$$t = 90^o - \arctan(\frac{-7.753}{\sqrt{(-24.080)^2 + (-44.513)^2}}) = 98.71^o \tag{5-19}$$

Then, we set up a virtual camera based on the position and orientation calculated in 3ds Max® (Fig. 5-18). The right bottom window of Fig. 5-18 shows the virtual photo generated by the virtual camera in 3ds Max®.

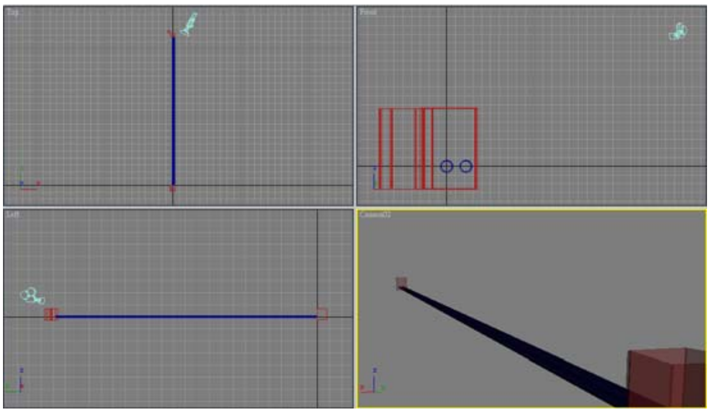

Fig. 5-18 The virtual camera with the virtual photo generated in 3ds Max®

To augment the 3D tunneling model into the site photo, the photo-augmenting equations need to be determined. The computed rotation matrix by Eq. (5-6b) is as:

$$M = \begin{bmatrix} 0.879550 & -0.475806 & 0.000000 \\ -0.072050 & -0.133189 & 0.988468 \\ -0.470319 & -0.869407 & -0.151428 \end{bmatrix}. \tag{5-20}$$

As the focal length f of the camera is equal to 18mm, we have the photo-augmenting equations of this application as:

$$\begin{aligned} x_n &= \frac{-15.8319X_n + 8.56451Y_n - 1622.70}{-0.470319X_n - 0.869407Y_n - 0.151428Z_n + 222.340}, \\ y_n &= \frac{1.29691X_n + 2.39739Y_n - 17.7924Z_n - 339.899}{-0.470319X_n - 0.869407Y_n - 0.151428Z_n + 222.340}. \end{aligned} \tag{5-21}$$

The center of one end of the electrical cable tunnel model is the origin of the local coordinates system, and the centre of the other end has the coordinates of (0, 218, 0). By Eq. (5-21), the image coordinates of the two points were calculated as (-7.298, -1.529) and (7.448, 5.570) respectively (unit: mm); note the origin of the 2D coordinate system in the photo falls on the center of the image plane. The simulated virtual photo was immersed into the real site photo shown as Fig. 5-19. Fig. 5-19 illustrates the effect of the augmented site photo, turning the jacking pit and concrete sleeve pipe visible. Fig. 5-19 also verifies the positions of the two calculated image points qualitatively.

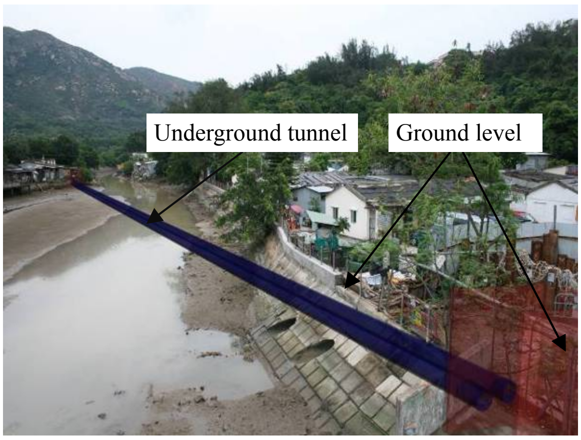

Fig. 5-19 The augmented photo with jacking pit and concrete sleeve pipes

The augmented photo was further attached with time dimensions to display the construction progress on site. In practice, the length of the installed tunnel could be measured directly by counting the number of pipe segments being jacked. The as-built progress of the construction thus could be visualized conveniently by using time stamped pipe jacking records to decide the cumulative tunnel length. As to the electrical cable tunnel, the total construction duration was 66 days and the total length was approximately 217m. The progress was visualized based on the augmented photos shown in Fig. 5-20.

Day 11, length of tunnel is 130m | Day 22, length of tunnel is 170m | Day 33, length of tunnel is 183m

Day 44, length of tunnel is 198m | Day 55, length of tunnel is 203m | Day 66, length of tunnel is 217m

Fig. 5-20 Construction progress visualization

5.6 SUMMARY

This chapter proposed an analytical approach by which the computer-generated graphics of invisible underground infrastructure can be augmented into the site photos. Notwithstanding the site photos contain valuable information for site engineers to evaluate the building quality and record project progress over time, the proposed methodology may help extend the use of site photos for construction progress visualization of underground infrastructure.

The proposed approach simplified the process of determining the camera's orientations by measuring the coordinates of only two reference points, namely, the camera station position and the object focus position. By simulating the image forming process of the camera, the research has developed a method for taking virtual photographs of the underground infrastructure and analytically overlaying the virtual photographs onto the real site photos. The method is computationally simple and holds great potential for achieving automation for engineering applications. The setup of the method is also easy-to-apply, suitable for construction engineers to follow and implement on site.

In this research, there are two main factors that influence the registration accuracy of the augmented photos, namely, the achievable surveying accuracies on the camera station position and the object focus position, and the systematic error due to imperfection of the camera. The properties of the camera system that affect the registration accuracy include the lens distortion, the displacement of the principal points (x_o, y_o) on the image plane, and the principal length being approximated by the focal length ($c \approx f$). Evaluating the error induced by the camera system entails fixing the focal length of the camera lens and imposing restrictions on the shooting distance between the lens and the object. As such, the registration accuracy varies with different camera settings. Specifically in conducting case studies for this research, the camera settings of a Canon EOS 400D are: the focal length of 18 mm, the shooting distance being within 50 m. The theoretical calculation based on the camera's internal components evaluates the shift of the virtual axes on the camera image plane to be in order of 0.06 mm. The control points were surveyed by a high-precision total station with a surveying error of 2-3 mm (standard deviation) on point coordinates. It adds an extra transfer error of 0.01 mm on the camera image plane. In this specific case, the internal error and surveying error are independent, so adding up the two error components results in an overall registration accuracy level of 0.07 mm.

The level of accuracy on the camera image plane can be further transformed onto the display device (i.e. monitor) based on the specific device model and setting applied. Given the camera CCD size of 22.2 × 14.8 mm and resolution of 3888 × 2592 pixels in this research, if the augmented photo is displayed on a desktop monitor with 17 inches in size and 1280 × 1024 pixels in screen resolution, the real and virtual axes will have a discrepancy level of 3.2 mm. If a laptop with the screen size in 14 inches and resolution in 1024 × 768 pixels is chosen, the level of discrepancy will be 3.4 mm. The evaluated accuracies both satisfy the needs of practical applications in the present research (i.e. underground infrastructure investigation and progress visualization). Additionally, the case studies intuitively have revealed the satisfactory registration effect in applying the photo-augmenting method in the bored pile excavation and micro-tunneling applications.

In short, the above case studies indicate the sufficiency of the registration accuracy for the photo-augmenting method in addressing the application needs for quality check and progress visualization of infrastructure engineering. Nonetheless, it should be pointed out that the actual registration accuracy should be meticulously investigated for a particular application that demands accurate registration.

CHAPTER 6

CONCLUSIONS

6.1 INTRODUCTION

The last chapter summarizes the research contributions in both academic and practical aspects and addresses research limitations and recommendations for future extensions.

6.2 SUMMARY OF WORK

The photogrammetry boasts the advantages of as-built reality capture, non-contact quantity surveying, and cost-effective yet convenient instrumental setup, lending itself well to improving construction managerial and operational practices. So far, construction professionals involved in photogrammetry applications have not attached much importance to the fundamental mathematics underlying this technique. This partially accounts for the fact that the capabilities of photogrammetry have not yet to be fully harnessed in construction. This research has studied the analytics of photogrammetry and made an attempt to turn the merits of photogrammetry into the systematic solutions in three application areas in construction. The basic research flow is to use “photo” data for mapping from 2D perceptions to 3D objects, accuracy quantification of the mapping results, and converting 3D object models onto 2D virtual views for site photo augmentation.

The first part of the research is a characterization of the basic algebraic mathematics of photogrammetry and applications of photogrammetry to model three-dimensional as-built building products and elements on site. Rays of light from the surface of an object in the 3D space are projected onto the image plane of a camera, generating a 2D image of the 3D scene. Photogrammetry is capable of extracting data from the 2D images and mapping them onto the 3D space by translating point coordinates in a 2D coordinate system into a 3D coordinate system. The research has investigated the mathematics underlying the analytical process, based on which, a 3D modeling method is proposed to use two photos taken from different perspectives to fix coordinates of any point in the 3D space. The method utilizes five paired image points to calculate the camera’s position and orientation. As such, the 3D models for site objects could be sketched from multiple site pictures without the needs for setting up the tripod and measuring the absolute coordinates of the camera and control points. Applying the developed modeling procedure under practical constraints was demonstrated with a practical case of a precast façade.

The second part has developed an analytical technique for assessment of the accuracy of applying photogrammetry to take geometric measurements on building products. Two major factors account for errors in the geometric measurements resulting from photogrammetry, namely: (1) the systematic error due to distortion of the camera lens, and (2) the random error due to human factors. The twelve objects sampled in the experiments were building products and building facilities found on the campus of Hong Kong Polytechnic University, yielding seventy-nine paired geometric measurements (length, width, and height) by photogrammetry and by measurement tape respectively. The "95% limits of agreement" method is applied on the sample data and the confidence intervals are established for the limits of agreement derived, so as to ensure validity and statistical significance of the results. By weighing the accuracy level achievable by photogrammetry against the accuracy level desirable in a particular application, the engineer can make the final decision on the applicability of the photogrammetry-based approach.

The third part is an investigation of adapting photogrammetric analytics to augmented reality (AR) applications in construction engineering. The rotation angles describing a camera's position in the 3D space in terms of azimuth (α), tilt (t), and swing (s) are introduced and the photo-augmenting equations are developed, by which site photos could be analytically combined with computer-generated 3D graphics of invisible underground infrastructure. The proposed approach simulates the imaging process of a camera and produces a virtual photo of the underground scene. As the virtual coordinate axes coincide with the real coordinate axes of the aboveground site scene, the virtual photo and the site photo are seamlessly merged in terms of perspective, position, and scale. The research has simplified the camera's spatial orientation determination by use of the positions of only two reference points, i.e. the camera station position and the object focus position. The level of accuracy for augmented photo registration depends on the specific implementation settings, including the point surveying instrument applied and the camera used. As for the bored pile excavation and micro-tunneling cases conducted in this research, given the exact coordinates of the camera station position and the object focus position, the augmented photo registration can achieve an accuracy level of 0.07 mm on the camera image plane. As a result, the whole procedure of the approach is computationally simple and practically applicable, which could be automated into a computer program. The proposed approach has been applied to superimpose as-built models of infrastructure onto site photos in order to facilitate quality check of bored pile excavation and progress visualization of micro-tunneling construction.

6.3 DISSERTATION CONTRIBUTIONS

6.3.1 Academic Contributions

As a cross-disciplinary study of surveying informatics and construction engineering and management (CEM), this research mainly contributes to the CEM domain. The surveying technique - photogrammetry has been applied in a wide range of disciplines including the construction discipline; this research continues with the exploration of the “nuts and bolts” of photogrammetry to make it better cater for construction applications.

The main contribution to knowledge is to explain and simplify analytical algorithms in terms and forms that are acceptable to CEM and conducive to problem solving in site photo related construction applications. These algorithms include the use of two photos for fixing the spatial point position, the use of image points for deriving the camera’s position and orientation, and photo-augmenting equations for merging site photos with as-built / as-designed 3D graphics, which are all straightforward and computationally simple. Furthermore, simplification has been made on how to derive camera perspective by use of two specified point positions by which to determine the camera position and orientation. This plays an important role in the successful registration of augmented photos and transformation of different sets of data into one coordinate system in the image space. In the actual fields, point coordinates are normally easier to measure than rotation angles. From this point of view, this research may promote the widespread use of photogrammetry and image processing in construction applications.

The other contribution to knowledge is the introduction of the statistical method - "95% limits of agreement" to evaluating two site measurement methods in terms of their interchangeability. This statistical method originates from medicine studies and has been widely applied in evaluation of replaceable medical apparatus. In this research, the "95% limits of agreement" method is applied for assessing the discrepancy between geometric measurements taken on the same building products by photogrammetry and by measurement tape respectively, so as to establish the accuracy level of the photogrammetry-based measurement method. In a broader sense, the "95% limits of agreement" method is applicable to solve other problems of similar nature in construction research.

6.3.2 Application Contributions

As for the contributions to applications, this research yields three practical solutions with respect to (1) modeling the as-built site elements in support of 3D graphical simulation and laying the mathematical foundation for applying photogrammetry to check the quantities on as-built building products and measure the dimensions on prefabricated building elements for quality control, (2) quantitatively assessing the accuracy level of applying photogrammetry to take measurements on dimensions of building products and site elements, and (3) augmenting the site photo with the invisible underground infrastructure graphics to generate a full view including both ground and underground site situations for better site visualization and investigation.

The photo-based 3D modeling method is analytically formulated and validated through experiments, aimed to support the visualization of construction operations simulation. Behzadan and Kamat (2007) introduced the augmented reality (AR) technique for the graphical construction simulation by setting the real images captured as the background scene for the visualization and incorporating the animated CAD / VR models of leading resources and equipment such as tower crane and backhoe into the real images. However, the engineers need provide the model ingredients for the animation, and preparing those models could be labor-intensive and time-consuming. Often, the design drafts or geometry specifications of the modeling objects are unavailable or the modeling objects are inaccessible for direct measurement due to safety concerns. On the other hand, visualizing the simulation does not require the models to be built with high accuracy. Thus, the photo-based method serves as a 3D modeling alternative by processing the image data contained in site photos, substantially saving the modeling time and effort. The practical site constraints are also taken into account in the field implementation of the proposed method.

The accuracy assessment study compares the photogrammetry-derived measurement method with the conventional tape measurement method, and statistically determines their degree of agreement. The results are statistically analyzed, producing the accuracy level of [-15.30 mm, 11.39 mm] in terms of the 95% limits of agreement. The main conclusion is that photogrammetry-derived geometric measurements could be used interchangeably in particular applications of construction management. Such results are useful for practitioners to (1) survey the geometric measurements on building products and site elements situated in hazard areas that are unsafe to access if the conventional tape measurement method is applied, and (2) quickly check the dimensions on prefabricated building units prior to site erection for quality control purposes. Essentially, the photogrammetry-derived measurement method can replace the real measurements (tape measurements). Through weighing the accuracy level achievable by photogrammetry against the accuracy level desirable in a particular application, the engineer makes the final decision on the applicability of the photogrammetry-based approach.

The photo-augmenting approach analytically superimposes the computer-generated, 3D graphics of invisible underground infrastructure into the site photos. Such augmented photos contain more valuable information and provide a complete perception of the site situation when engineers want to check the quality of the underground facilities and evaluate the project progress over time. The proposed approach simplifies the field instrument setup as needed to determine the camera orientations in 3D space. In the present approach, only coordinates of two reference points, i.e. the camera station position and the object focus position are required to be measured, which, in large part, makes the method much easier for engineers to implement on site.

The photo-augmenting approach also potentially contributes to the augmented reality (AR) research in terms of registration in construction applications. *Registration* is a necessary step to materialize AR visualization, which means that the axes of the real and virtual coordinate systems are made to coincide in the three-dimensional (3D) augmented space (Barfield and Caudell 2001). This requires data on the current coordinates of the observer and rotation angles of the observer's perspective, which are continuously tracked and updated in real time. Current practice relies on the hardware tracking devices such as GPS, compass, gyroscope to fulfill this task (Kamat and El-Tawil 2007; Behzadan and Kamat 2007; Shin and Dunston 2009). The proposed approach holds the potential to determine the spatial angular orientations of the observer's perspective by only determining the coordinates of two particular points. Thus the registration of AR in terms of spatial rotation angles determination can be significantly simplified by calculation, considerably streamlining hardware installation in implementing AR applications in a construction field.

6.4 RECOMMENDATIONS AND FUTURE EXTENSIONS

A possible extension of the present study is to increase the level of automation for the photo-based 3D modeling method by looking into techniques for identification and referencing of object features based on photos, which are being rapidly advanced in the research area of computer vision. Though the accuracy has yet to satisfy the engineering needs, a number of research developments in computer vision have already addressed automated reconstruction of models from photos, including unsupervised 3D object recognition and reconstruction (Brown and Lowe 2005), internet photo collection based modeling (Snavely et al. 2008), video-based real time urban 3D modeling (Pollefeys et al. 2008), and four dimensional augmented reality (Golparvar-Fard et al. 2009). These techniques might be adapted to substantially automate the process of recognizing and matching the corners and edges of prefabricated units and building products based on processing site photos. To extend the present research, the future work will learn from the above techniques to explore if they can be applied to improve the proposed methods for construction applications. In addition, specific computer vision algorithms will be investigated to enable the computer system to automatically recognize feature points on images, reference corresponding points across different images, and filter noises in connection with any mismatches. These algorithms include scale invariant feature transforms (SIFT; Lowe 2004), combined corner and edge detector (Harris and Stephens 1988), point feature detector and tracker (Tomasi and Kanade 2004), speeded up robust features (SURF; Bay et al. 2006), and scale and affine invariant point detector (Mikolajczyk and Schmid 2004).

A natural extension of the present study is to quantitatively formalize the relationship between major factors that affect the photogrammetry accuracy for taking geometric measurements on building products and site elements. In the present research, the camera setting is restricted to (1) using Canon EOS 400D (10 mega pixels), (2) focal length set to 18mm, and (3) shooting range in [1m, 6m]. This lacks flexibility as application condition changes. Recent research and experiments have revealed: The higher the camera resolution, the better accuracy photogrammetry achieves (Cleveland and Wartman 2006); the focal length of the camera determines the view angle, and a wider angle resulting from a smaller focal length may undermine the accuracy; and the longer the shooting distance between the camera station and the imaging object, the lower the accuracy of the photogrammetry measurement. But how will the camera resolution, the focal length, and the shooting distance jointly affect the resulting accuracy? The answer can serve as the guidance for engineers to choose camera configurations when they want to use photogrammetry to measure a building product under different photographing conditions. The analytical relationship has not been developed yet. This will be the follow up research direction in the future.

Another extension may relate to the realization of the photo-based augmented reality method. Successful implementation of the proposed method may take into consideration the coordinates and pixel mapping between the image plane of the camera and the screen of the display device (e.g., LCD). The coordinates are metrically presented, while in digital imaging, the pixel is the smallest item of information in the image (Graf 1999). The pixel does not have coherent fixed metric dimension in size and usually is device-dependant. How to achieve the practical conversion between metrics and pixels should be addressed in the future research.

6.5 CHAPTER SUMMARY

The last chapter serves as the synopsis of the whole dissertation. A thorough review of the research is given, followed by a summary of the academic and application contributions achieved. Last, limitations of the research and recommendations for future extensions are discussed.

APPENDIX I

THE PRINCIPAL DISTANCE APPROXIMATION

The principal distance (c) of a camera in photography is defined as the distance of the perpendicular line from the perspective center (center of lens opening) to the image plane of the camera. c equals the image distance v when the image plane is at the exact position along the optical axis that clear object is focused. Under such circumstances, the distance between the object and camera lens opening is denoted by object distance u. Fig. I-1 illustrates the object distance and the image distance when photographing an object.

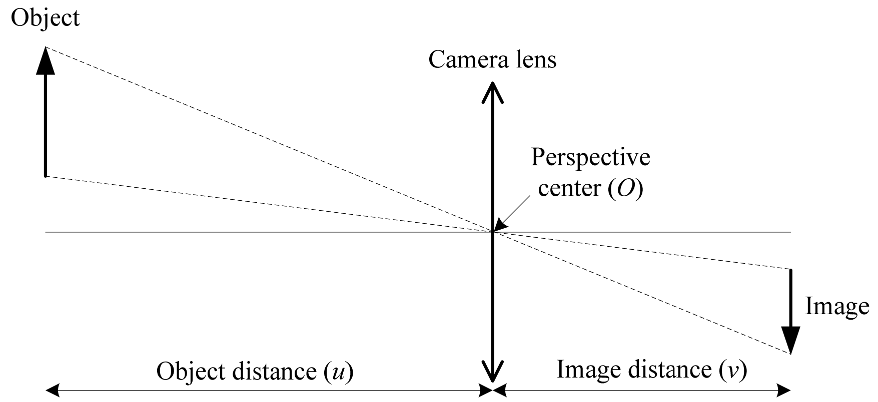

Fig. I-1 Illustrated object distance and image distance

The conjugated distances of u, v and the focal length f are related by the *lens conjugate equation* (Ray 1984) as:

$$\frac{1}{u}+\frac{1}{v}=\frac{1}{f}. \tag{I-1}$$

by which the focal length can be derived by:

$$f=\frac{uv}{u+v}. \tag{I-2}$$

In reality of photography, the object distance u is much farther than the image distance v. As such, the denominator $u+v$ can be approximated as u, which consequently yields:

$$f \approx v. \tag{I-3}$$

This proves the assertion that the *principal distance* (c) can be practically approximated to the focal length of the camera lens when focused at infinity, namely, $c \approx f$.

APPENDIX II

PARTIAL DERIVATIVES OF COPLANARITY EQUATION

The coplanarity equation of Eq. (3-6) is represented in a form of determinant of a 3 ×3 matrix, which can be calculated as in Eq. (II-1):

$$
\begin{aligned}
F &= \begin{vmatrix} e_{11} & e_{12} & e_{13} \\ e_{21} & e_{22} & e_{23} \\ e_{31} & e_{32} & e_{33} \end{vmatrix} \\
&= e_{11}\begin{vmatrix} e_{22} & e_{23} \\ e_{32} & e_{33} \end{vmatrix} - e_{12}\begin{vmatrix} e_{21} & e_{23} \\ e_{31} & e_{33} \end{vmatrix} + e_{13}\begin{vmatrix} e_{21} & e_{22} \\ e_{31} & e_{32} \end{vmatrix} \\
&= e_{11}(e_{22}e_{33} - e_{23}e_{32}) - e_{12}(e_{21}e_{33} - e_{23}e_{31}) + e_{13}(e_{21}e_{32} - e_{22}e_{31}).
\end{aligned}
\tag{II-1}
$$

where e_{ij} is the elements of the 3 ×3 matrix. Correspondingly, the partial derivative of Eq. (3-6) with respect to a parameter p can be calculated as in Eq. (II-2):

$$
\frac{\partial F}{\partial p} = \begin{vmatrix} \frac{\partial e_{11}}{\partial p} & \frac{\partial e_{12}}{\partial p} & \frac{\partial e_{13}}{\partial p} \\ e_{21} & e_{22} & e_{23} \\ e_{31} & e_{32} & e_{33} \end{vmatrix} + \begin{vmatrix} e_{11} & e_{12} & e_{13} \\ \frac{\partial e_{21}}{\partial p} & \frac{\partial e_{22}}{\partial p} & \frac{\partial e_{23}}{\partial p} \\ e_{31} & e_{32} & e_{33} \end{vmatrix} + \begin{vmatrix} e_{11} & e_{12} & e_{13} \\ e_{21} & e_{22} & e_{23} \\ \frac{\partial e_{31}}{\partial p} & \frac{\partial e_{32}}{\partial p} & \frac{\partial e_{33}}{\partial p} \end{vmatrix}.
\tag{II-2}
$$

Thus, the partial derivatives of F with respect to the five unknowns $Y_{o'}, Z_{o'}, \omega^{'}$, $\phi^{'}, \kappa^{'}$ in Eq. (3-9) are calculated as:

$$\frac{\partial F}{\partial Y_{o'}} = -\begin{vmatrix} x_p - x_o & -c \\ u & w \end{vmatrix}. \tag{II-3}$$

$$\frac{\partial F}{\partial Z_{o'}} = \begin{vmatrix} x_p - x_o & y_p - y_o \\ u & v \end{vmatrix}. \tag{II-4}$$

$$\frac{\partial F}{\partial \omega^{'}} = \begin{vmatrix} X_{o'} & Y_{o'} & Z_{o'} \\ x_p - x_o & y_p - y_o & -c \\ \partial u / \partial \omega^{'} & \partial v / \partial \omega^{'} & \partial w / \partial \omega^{'} \end{vmatrix}, \tag{II-5}$$

where

$$\begin{aligned} &\partial u / \partial \omega^{'} = 0, \\ &\partial v / \partial \omega^{'} = (x_p^{'} - x_o)(\cos\omega^{'} \sin\phi^{'} \cos\kappa^{'} - \sin\omega^{'} \sin\kappa^{'}) - \\ &\qquad (y_p^{'} - y_o)(\cos\omega^{'} \sin\phi^{'} \sin\kappa^{'} + \sin\omega^{'} \cos\kappa^{'}) + c\cos\omega^{'} \cos\phi^{'}, \\ &\partial w / \partial \omega^{'} = (x_p^{'} - x_o)(\sin\omega^{'} \sin\phi^{'} \cos\kappa^{'} + \cos\omega^{'} \sin\kappa^{'}) - \\ &\qquad (y_p^{'} - y_o)(\sin\omega^{'} \sin\phi^{'} \sin\kappa^{'} - \cos\omega^{'} \cos\kappa^{'}) + c\sin\omega^{'} \cos\phi^{'}. \end{aligned} \tag{II-6}$$

$$\frac{\partial F}{\partial \phi^{'}} = \begin{vmatrix} X_{o'} & Y_{o'} & Z_{o'} \\ x_p - x_o & y_p - y_o & -c \\ \partial u / \partial \phi^{'} & \partial v / \partial \phi^{'} & \partial w / \partial \phi^{'} \end{vmatrix}, \tag{II-7}$$

where

$$
\begin{aligned}
\partial u / \partial \phi^{'} &= -(x_p^{'} - x_o)\sin\phi^{'}\cos\kappa^{'} + (y_p^{'} - y_o)\sin\phi^{'}\sin\kappa^{'} - c\cos\phi^{'}, \\
\partial v / \partial \phi^{'} &= (x_p^{'} - x_o)\sin\omega^{'}\cos\phi^{'}\cos\kappa^{'} - \\
&\quad (y_p^{'} - y_o)\sin\omega^{'}\cos\phi^{'}\sin\kappa^{'} - c\sin\omega^{'}\sin\phi^{'}, \\
\partial w / \partial \phi^{'} &= -(x_p^{'} - x_o)\cos\omega^{'}\cos\phi^{'}\cos\kappa^{'} + \\
&\quad (y_p^{'} - y_o)\cos\omega^{'}\cos\phi^{'}\sin\kappa^{'} + c\cos\omega^{'}\sin\phi^{'}.
\end{aligned} \tag{II-8}
$$

$$
\frac{\partial F}{\partial \kappa^{'}} = \begin{vmatrix} X_{o'} & Y_{o'} & Z_{o'} \\ x_p - x_o & y_p - y_o & -c \\ \partial u / \partial \kappa^{'} & \partial v / \partial \kappa^{'} & \partial w / \partial \kappa^{'} \end{vmatrix}, \tag{II-9}
$$

where

$$
\begin{aligned}
\partial u / \partial \kappa^{'} &= -(x_p^{'} - x_o)\cos\phi^{'}\sin\kappa^{'} - (y_p^{'} - y_o)\cos\phi^{'}\cos\kappa^{'}, \\
\partial v / \partial \kappa^{'} &= -(x_p^{'} - x_o)(\sin\omega^{'}\sin\phi^{'}\sin\kappa^{'} - \cos\omega^{'}\cos\kappa^{'}) - \\
&\quad (y_p^{'} - y_o)(\sin\omega^{'}\sin\phi^{'}\cos\kappa^{'} + \cos\omega^{'}\sin\kappa^{'}), \\
\partial w / \partial \kappa^{'} &= (x_p^{'} - x_o)(\cos\omega^{'}\sin\phi^{'}\sin\kappa^{'} + \sin\omega^{'}\cos\kappa^{'}) + \\
&\quad (y_p^{'} - y_o)(\cos\omega^{'}\sin\phi^{'}\cos\kappa^{'} - \sin\omega^{'}\sin\kappa^{'}).
\end{aligned} \tag{II-10}
$$

APPENDIX III

CAMERA CALIBRATION FOR PHOTOGRAMMETRY APPLICATION

The camera used in this experiment was the off-the-shelf digital single lens reflection (DSLR) camera - Canon EOS 400D with the focal length set at 18 mm to obtain the widest shooting range of the camera. The calibration tool selected was a well-established commercial software system - PhotoModeler® (Eos Systems Inc. 2007), which prevails both in the industrial markets and in the research fields. The calibration is to determine the camera's interior parameters in terms of focal length, displacement of principal point, and the lens distortion.

The calibration usually involves two steps: (1) taking the calibration photos, and (2) deriving the camera parameters with those photos. As Fig. III-1 shows, eight photos of a calibration grid are recommended to be taken from four edges of the grid with a combination of portrait orientation and landscape orientation. The camera focal length needs to be kept constant during the entire course of photo taking. Here, the calibration grid is a pattern of dots designed specifically for the Camera Calibrator in

PhotoModeler®, and the Camera Calibrator is a computer program running on the algorithm for automation of the derivation of camera parameters.

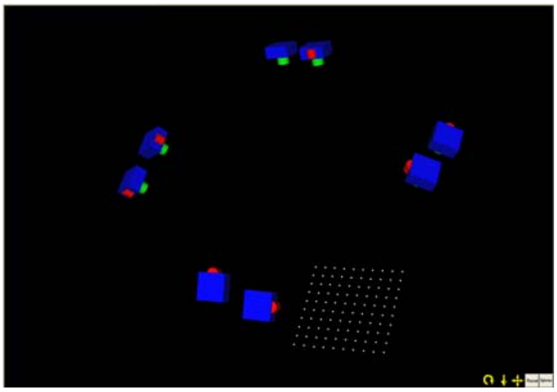

Fig. III-1 Eight camera locations derived in PhotoModeler® as part result of the camera calibration

The calibration results include the radial lens distortion parameters (K_1 = 5.167e-004, K_2 = -1.120e-006), the decentering lens distortion parameters (P_1 = 3.924e-005, P_2 = 3.684e-005), the image coordinates of the principal point (x_o = 11.1042 mm, y_o = 7.5231 mm), and the adjusted focal length (f = 18.0562 mm). The threshold for evaluating the quality of the calibration results is defined as the maximum residual being less than one pixel (PhotoModeler User's Manual 2004). In this research, the calibration results have the maximum residual of 0.2095 pixel, indicating a good calibration of the camera parameters.

Note, the calibration work is only needed in the first time of using the camera to take source photos. As long as the focal length does not change, successive modeling work can use the same calibration results to determine the internal camera parameters.

APPENDIX IV

THE STANDARD ERROR OF 95% LIMITS OF AGREEMENT

The standard error of the 95% limits of agreement can be denoted by: $\sqrt{Var(\bar{X} \pm 1.96S)}$, where $\bar{X}$ is the random variable of the sample mean, S is the random variable of the sample standard deviation.

As $\bar{X}$ and S are independent, $Var(\bar{X} \pm 1.96S)$, which is the variance of the 95% limits of agreement, can be written as:

$$Var(\bar{X} \pm 1.96S) = Var(\bar{X}) + 1.96^2 Var(S) \tag{IV-1}$$

The $Var(\bar{X})$ is σ^2 / n, and approximated to s^2 / n. To determine $Var(S)$, we firstly derive the expected value and variance of S^2, i.e. $E[S^2]$ and $Var(S^2)$, by calculating the expected value and variance of $\sigma^2 \chi^2_{n-1} /(n-1)$ on the grounds that S^2 is distributed as the statistic $\sigma^2 \chi^2_{n-1} /(n-1)$ (χ^2_{n-1} is the *Chi-square distribution* with $n-1$ degrees of freedom). According to Rohatgi (1976), the expected value and variance of χ^2_{n-1} are denoted by:

$$\begin{aligned} &E[\chi^2_{n-1}] = n-1 \\ &Var(\chi^2_{n-1}) = 2(n-1) \end{aligned} \tag{IV-2}$$

Thus:

$$\begin{aligned} &E[S^2] = E[\sigma^2 \chi^2_{n-1} /(n-1)] = \sigma^2 \\ &Var(S^2) = Var(\sigma^2 \chi^2_{n-1} /(n-1)) = 2\sigma^4 /(n-1) \end{aligned} \tag{IV-3}$$

Then we employ the delta method (Oehlert 1992) to derive the variance of S. This method is to take second-order Taylor expansions to approximate the variance of a function of one or more random variables. Given X be a random variable with $E[X] = \mu_x$ and $Var(X) = \sigma_x^2$, then the approximate variance of a function of X is given by:

$$Var[f(X)] \approx [\frac{d}{dX} f(X)\Big|_{\mu_x}]^2 \times \sigma_x^2 \tag{IV-4}$$

provided that f is twice differentiable and that the mean and variance of X are finite. Let $f(X) = \sqrt{X}$, Eq. (IV-4) becomes:

$$\begin{aligned} Var(\sqrt{X}) &\approx [\frac{d}{dX}\sqrt{X}\Big|_{\mu_x}]^2 \times \sigma_x^2 \\ &= [\frac{1}{2\sqrt{X}}\Big|_{\mu_x}]^2 \times \sigma_x^2 \\ &= \frac{\sigma_x^2}{4\mu_x} \end{aligned} \tag{IV-5}$$

Let $X = S^2$, and denote μ_x, σ_x^2 in Eq. (IV-5) by Eq. (IV-3), we have:

$$Var(S) = Var(\sqrt{S^2}) = \frac{\sigma^2}{2(n-1)} \qquad \text{(IV-6)}$$

To use s^2 to represent σ^2, we finally approximate $Var(S)$ by $s^2 / 2(n-1)$.

Now put the formulae of $Var(\bar{X})$ and $Var(S)$ back into Eq. (IV-1):

$$\begin{aligned} Var(\bar{X} \pm 1.96S) &= Var(\bar{X}) + 1.96^2 Var(S) \\ &= \frac{s^2}{n} + 1.96^2 \frac{s^2}{2(n-1)} \\ &= (\frac{1}{n} + \frac{1.96^2}{2(n-1)})s^2 \end{aligned} \qquad \text{(IV-7)}$$

When n is large, let $n-1 \approx n$, this equation can be approximated into $2.92s^2 / n$. Hence, standard errors of $\bar{X} - 1.96S$ and $\bar{X} + 1.96S$ are approximated as $1.71s / \sqrt{n}$. Thus, the standard error for the 95% limits of agreement can be estimated in Eq. (4-7).

APPENDIX V

STATISTICAL SYMBOLS USED IN CHAPTER 4

$\bar{x} = \frac{1}{n}\sum_{i=1}^{n} x_i$, the sample mean of a sample $x_1, x_2, \ldots, x_n$

$s^2 = \frac{1}{n-1}\sum_{i=1}^{n}(x_i - \bar{x})^2 = \frac{1}{n-1}(\sum_{i=1}^{n} x_i^2 - n\bar{x}^2)$, the sample variance of a sample

$s = \sqrt{s^2}$, the sample standard deviation

μ , the mean of the whole population

σ^2 , the variance of the whole population

$\bar{X}$, the random variable of the sample mean

S , the random variable of the sample standard deviation

$E[X]$, the expected value / mean of the random variable X

$Var(X)$, the variance of the random variable X

χ^2_{n-1} , the statistic of the *t*-distribution with $n-1$ degrees of freedom

REFERENCES

Abdel-Aziz, Y.I., and Karara, H.M. (1971). "Direct linear transformation from comparator coordinates into object space coordinates in close-range photogrammetry." *Proceedings of the ASP/UI Symposium on Close-Range Photogrammetry*, 1-18. Univ. of Illinois, Urbana, IL.

Abeid, J., Allouche, E., Arditi, D., and Hayman, M. (2003). "PHOTO-NET II: A computer based monitoring system applied to project management." *Automation in Construction*, 12(5), 603-616.

Abeid, J.N., and Arditi, D. (2002a). "Linking time-lapse digital photography and dynamic scheduling of construction operations." *Journal of Computing in Civil Engineering*, ASCE, 16 (4), 269–279.

Abeid, J.N., and Arditi, D. (2002b). "Time-lapse digital photography applied to project management." *Journal of Construction Engineering and Management*, 128(6), 530–535.

Akinci, B., Fischer, M., Levitt, R., and Carlson, B. (2002). "Formalization and automation of time-space conflict analysis." *Journal of Computing in Civil Engineering*, ASCE, 6(2), 124-135.

Akinci B., Boukamp F., Gordon C., Huber D., Lyons C., and Park K. (2006). "A formalism for utilization of sensor systems and integrated project models for active construction quality control." *Automation in Construction*, 15(2), 124-138.

Al-Hussein, M., Niaz, M.A., Yu, H., and Kim, H. (2006). "Integrating 3D visualization and simulation for tower crane operations on construction sites." *Automation in Construction*, 15(5), 554-562.

Almagro, A., Patias, P., and Waldhausl, P. (1996). "The CIPA 'Wagner Pavilion' test." *International Archives of Photogrammetry and Remote Sensing*, 31(B5), 463-469.

Altman, D.G., and Bland, J.M. (1983). "Measurement in medicine - the analysis of method comparison studies." *Statistician*, 32(3), 307-317.

Arias, P., Ordonez, C., Lorenzo, H., Herraez, J., and Armesto, J. (2006). "Low-cost documentation of traditional agro-industrial buildings by close-range photogrammetry." *Building and Environment*, 42(4), 1817-1827.

Autodesk. (2009). "3ds Max: Production-proven 3D modeling, animation, and rendering solution for entertainment and engineering application." <http://usa.autodesk.com/adsk/servlet/index?siteID=123112&id=5659302> (March 2, 2009).

Autodesk. (2007). "AutoCAD: Computer-aided design software targeting easy, convenient and fast drafting and modeling for the industries." <http://usa.autodesk.com/adsk/servlet/pc/index?id=13779270&siteID=123112> (accessed June 10, 2007).

Barfield, W., and Caudell, T. (2001). *Fundamentals of wearable computers and augmented reality*, Erlbaum, Mahwah, N.J.

Bay, H., Tuytelaars, T., and Gool, L.V. (2006). "SURF: Speeded Up Robust Features". *Proceedings of the 9th European Conference on Computer Vision*, Springer LNCS volume 3951, part 1. pp. 404-417.

Behzadan, A.H., and Kamat, V.R. (2007). "Georeferenced Registration of Construction Graphics in Mobile Outdoor Augmented Reality", *Journal of Computing in Civil Engineering*, ASCE, 21(4), 247-258.

Beyer, H.A., Uffenkamp, V., and van der Vlugt, G. (1995). “Quality control in industry with digital photogrammetry.” *Optical 3-D Measurement Techniques III*, eds. A. Gruen and H. Kahmen, Wichmann Verlag, Heidelberg, 29-38.

Blachut, T.J., and Burkhardt, R. (1989). *Historical development of photogrammetric methods and instruments*, ASPRS, Falls Church, VA, Chap. 1, 4-18.

Bland, J.M., and Altman, D.G. (1986). “Statistical-methods for assessing agreement between 2 methods of clinical measurement.” *Lancet*, 1(8476), 307-310.

Bland, J.M., and Altman, D.G. (1995). “Comparing methods of measurement - why plotting difference against standard method is misleading.” *Lancet*, 346(8982), 1085-1087.

Bland, J.M., and Altman, D.G. (1999). “Measuring agreement in method comparison studies.” *Statistical Methods in Medical Research*, 8(2), 135-160.

Bland, J.M, and Altman, D.G. (2003). “Applying the right statistics: analyses of measurement studies.” *Ultrasound in Obstetrics & Gynecology*, 22(1), 85-93.

Brilakis, I, and Soibelman, L. (2005). “Content-based search engines for construction image databases.” *Automation in Construction*, 14(4), 537-550.

Brown, D.C. (1966). “Decentering distortion of lenses.” *Photogrammetric Engineering*, 32(3), 444-462.

Brown, M., and Lowe, D.G. (2005). "Unsupervised 3D object recognition and reconstruction in unordered datasets," *International Conference on 3-D Digital Imaging and Modeling (3DIM 2005)*, June, Ottawa, Canada.

Burke, P.H., and Beard, L.F.H. (1979). "Growth of soft tissues of the face in adolescence." *British Dental Journal*, 146(8), 239-246.

Chikatsu, H., Turuoka, M., and Murai, S. (1992). "Sports dynamics of Carl Lewis through 100 m race using video imagery." *International Archives of Photogrammetry and Remote Sensing*, 29(B5), 875– 879.

Cleveland, J.L., and Wartman, J. (2006). "Principles and applications of digital photogrammetry for geotechnical engineering." *Site and Geomaterial Characterization: Proceedings of Sessions of GeoShanghai*, eds. Anand J. Puppala, Dante Fratta, Khalid Alshibli, and Sibel Pamukcu, June 6-8, 2006, Shanghai, China, 128-135. Reston, VA: ASCE/GEO Institute.

Coombes, A.M., Linney, A.D., Richards, R., and Moss, J.P. (1990). "A method for the analysis of the 3D shape of the face and changes in the shape brought about by facial surgery." In: Herron, R. E. (Ed.), *Biostereometric Technology and Applications. Proc. SPIE*, 1380, 180-189.

Dare, P., Hanley, H., Fraser, C., Riedel, B., and Niemeier, W. (2002). "An operational application of automatic feature extraction: the measurement of cracks in concrete structures." *The Photogrammetric Record*, 17(99), 453-464.

Dewitt, B.A. (1996). "Initial approximations for the three-dimensional conformal coordinate transformation." *Journal of Photogrammetric Engineering and Remote Sensing*, 62(1), 79-83.

Dunston, P.S., and Wang, X. (2005). "Mixed reality-based visualization interfaces for architecture, engineering, and construction industry." *Journal of Construction Engineering and Management*, ASCE, 131(12), 1301-1309.

Eos Systems Inc. (2004). *User Manual for PhotoModeler® Pro Version 5*, Vancouver, BC.

Eos Systems Inc. (2007). “PhotoModeler: Close-range photogrammetric measurement and 3D modeling software.” <http://www.photomodeler.com> (June 20, 2007).

Fenton, S., and Ziernicki, R.M. (1999). “Using digital photogrammetry to determine vehicle crush and equivalent barrier speed (EBS).” *International Congress and Exposition - Session: Accident Reconstruction (Part C&D)*, March 1999, Detroit, MI, USA, 1999-01-0439.

Fraser, C.S. (1996). “Industrial measurement applications.” *Close Range Photogrammetry and Machine Vision*, Ed. K.B. Atkinson, Whittles, Scotland, Chap. 12, 329-361.

Fraser, C.S. and Riedel, B. (2000). “Monitoring the thermal deformation of steel beams via vision metrology.” *Journal of Photogrammetry & Remote Sensing*, ISPRS, 55(4), 268-276.

Golparvar-Fard, M., and Peña-Mora, F. (2007). “Development of visualization techniques for construction progress monitoring.” *Proc., ASCE Int. Workshop on Computing in Civil Eng*, Pittsburgh, PA.

Golparvar-Fard, M., Peña-Mora, F., and Savarese, S. (2009). “Application of D^{4}AR – A 4-dimensional augmented reality model for automating construction progress monitoring data collection, processing and communication.” *Journal of Information Technology in Construction*, vol. 14, 129-153.

Gould, F., and Joyce, N.E. (2002). *Construction Project Management*, 2nd ed., Prentice Hall, New Jersey.

Graf, R.F. (1999). *Modern Dictionary of Electronics*, 7th ed., Newnes, Oxford.

Halpin, D.W. (1977). “CYCLONE-method for modeling job site processes.” *J. Constr. Div.*, Am. Soc. Civ. Eng., 103(3), 489-499.

Halpin, D.W., and Riggs, L. (1992). *Planning and analysis of construction* *operations*, Wiley, New York.

Hampson, K., and Tatum, C.B. (1997). "Technology strategy and competitive performance in bridge construction." *Journal of Construction Engineering and Management*, ASCE, 123(2), 153-161.

Harris, C., and Stephens, M. (1988). "A combined corner and edge detector." *Proceedings of the 4th Alvey Vision Conference*, 147-151.

Jeong, H.S., and Abraham, D.M. (2004). "A decision tool for the selection of imaging technologies to detect underground infrastructure." *Journal of Tunneling and Underground Space Technology*, 19(2), 175-191.

Kamat, V.R., and El-Tawil, S. (2007). "Evaluation of augmented reality for rapid assessment of earthquake-induced building damage", *Journal of Computing in Civil Engineering*, ASCE, 21(5), 303-310.

Kamat, V.R., and Martinez, J.C. (2001). "Visualizing simulated construction operations in 3D." *Journal of Computing in Civil Engineering*, ASCE, 15(4), 329-337.

Kim, H., and Kano, N. (2008). "Comparison of construction photograph and VR image in construction progress." *Automation in Construction*, 17(2), 137-143.

Koo, B., and Fischer, M. (2000). "Feasibility study of 4D CAD in commercial construction." *Journal of Construction Engineering and Management*, ASCE, 126(4), 251-260.

Lee, S. and Peña-Mora, F. (2006). "Visualization of construction progress monitoring", *Proc. of Joint Int. Conf. on Computing and Decision Making in Civil & Building Engrg*, 2527-2533.

Linnet, K., and Bruunshuus, I. (1991). "HPLC with enzymatic detection as a candidate reference method for serum creatinine." *Clin. Chem.*, 37, 1669-1675.

Lowe, D. (2004). "Distinctive image features from scale-invariant keypoints." *International Journal of Computer Vision*, 60(2), 91-110.

Lu, M. (2003). "Simplified discrete-event simulation approach for construction simulation." *Journal of Construction Engineering and Management*, ASCE, 129(5), 537-546.

Lu, M., Dai, F., and Chen, W. (2007). "Real-time decision support for planning concrete plant operations enabled by integrating vehicle tracking technology, simulation, and optimization algorithms." *Canadian Journal of Civil Engineering*, 34(8), 912-922.

Luhmann, T., Robson, S., Kyle, S., and Harley, I. (2006). *Close Range Photogrammetry: Principles, Methods and Applications*, Whittles Publishing, Scotland, UK.

Luhmann, T., and Tecklenburg, W. (2001). "Hybrid photogrammetric and geodetic surveillance of historical buildings for an urban tunnel construction." *Proc., Int. Workshop on Recreating the Past Visualization and Animation of Cultural Heritage*, ISPRS, Enschede, The Netherlands.

Lynnerup, N., and Vedel, J. (2005). "Person identification by gait analysis and photogrammetry." *Journal of Forensic Sciences*, 50(1), 112-118.

Martinez, J.C., and Ioannou, P.G. (1999). "General-purpose systems for effective construction simulation." *Journal of Construction Engineering and Management*, ASCE, 125(4), 265-276.

McGlone, J. C. (1989). "Analytic data-reduction schemes in non-topographic photogrammetry." *Non-Topographic Photogrammetry*, 2nd ed., ed. H. M. Karara, ASPRS, Falls Church, VA, Chap. 4, 37–55.

McGlone, J.C., Mikhail, E.M., Bethel, J., and Mullen, R. (2004). *Manual of*

Photogrammetry, 5th ed. ASPRS.

McKinney, K., Kim, J., Fischer, M., and Howard, C. (1996). ‘‘Interactive 4D-CAD.’’ *Proc. 3rd Congr. on Comp. in Civ. Engrg.*, ASCE, New York, 383-389.

Memon, Z.A., Majid, M.Z.A., and Mustaffar, M. (2005). “An automatic project progress monitoring model by integrating AutoCAD and digital photos.” *Proceedings of the 2005 ASCE International Conference on Computing in Civil Engineering*, eds. L. Soibelman and F. Peña-Mora, Cancun, Mexico, p. 151.

Mikhail, E.M. (1976). *Observations and Least Squares*, IEP, New York.

Mikolajczyk, K., and Schmid, C. (2004). “Scale and affine invariant interest point detectors.” *International Journal of Computer Vision*, 60 (1), 63–86.

Mills, J.P., Newton, I., and Peirson, G.C. (2001). “Pavement deformation monitoring in a rolling load facility.” *The Photogrammetric Record*, 17(97), 07-24.

Mitchella, H.L., and Newton, I. (2002). “Medical photogrammetric measurement: overview and prospects.” *Journal of Photogrammetry and Remote Sensing*, ISPRS, 56(5-6), 286-294.

Moffitt, F.H., and Mikhail, E.M. (1980). *Photogrammetry*, 3rd ed., Harper & Row, New York.

Mok, E., King, B.A., Qing, Z., Li, Z.L., and Lam, K. (1998). “Digital close range digital photogrammetry data acquisition system with combined GPS georeference and its calibration.” *Proc., ISPRS Commission V Symposium Real-time Imaging and Dynamic Analysis*, June 2-5, Hakodate, Japan, vXXXII, n5, 253-257.

Moore, J.F.A. (1992). *Monitoring Building Structures*, Blackie and Sons Ltd., London, UK.

Oehlert, G.W. (1992). “A note on the delta method.” *The American Statistician*, 46(1), 27-29.

PhotoMetrix. (2007). “iWitness: The image-based 3D measurement tools for accident reconstruction.” <http://www.photometrix.com.au/products_i.html> (June 20, 2007).

Pollefeys, M. et al. (2008). “Detailed real-time urban 3D reconstruction from video.” *International Journal of Computer Vision*, 78(2-3), 143-167.

Proctor, D.W., and Atkinson, K.B. (1972). “Experimental photogrammetric wriggle survey in the Second Mersey Tunnel.” *Tunnels and Tunneling International*, 4(2), 115-118.

Przybilla, H.-J., Kotowski, R., Meid, A., and Weber, B. (1988). “Geometric quality control in nuclear power stations - a procedure for high precision underwater photogrammetry.” *International Archives of Photogrammetry and Remote Sensing*, 27(B5), 513-526.

Przybilla, H.-J., Meid, A., Kotowski, R., and Weber, B. (1990). “Geometrical quality control in nuclear power stations: an application of high precision underwater photogrammetry.” *The Photogrammetric Record*, 13(76), 577-589.

Quiñones-Rozo, C.A., Hashash, Y.M.A., and Liu, L.Y. (2008). “Digital image reasoning for tracking excavation activities.” *Automation in Construction*, 17(5), 608-622.

Ray, F.S. (1984). “Photographic optics.” *Photography for the Scientist*, 4th ed., ed. Morton, A. R., Academic Press Inc, Orlando, FL, Chap. 2, 104-124.

REALVIZ S.A. (2007). “ImageModeler: The image-based modeling and photogrammetry software that generates 3D models from 2D digital images.” <http://imagemodeler.realviz.com> (June 20, 2007).

Reichmann, W., and Ringel, H. (1995). “Photogrammetrische Verformungsanalysen in der Karosserie-Entwicklung.” *Tagung Optische Mebmethoden in der modernen Automobilentwicklung*, Haus der Technik, Essen.

Retik, A., and Shapira, A. (1999). “VR-based planning of construction site activities.” *Automation in Construction*, 8(6), 671-680.

Rüther, H. (1989). “An overview of software in non-topographic photogrammetry.” *Non-Topographic Photogrammetry*, 2nd ed., ed. H. M. Karara, ASPRS, Falls Church, VA, Chap. 10, 129-145.

Rohatgi, V. K. (1976). *An introduction to probability theory and mathematical statistics*, Wiley, New York.

Schneider, C.-T. (1994). “Einsatz der Industriephotogrammetrie im Schiffbau.” *Publikationen der DGPF*, Band 2, Augsburg 1993, 117-119.

Shih, T.Y. (1990). “The duality and critical condition in the formation and decomposition of a rotation matrix.” *Journal of Photogrammetric Engineering and Remote Sensing*, ASPRS, 56(8), 1173-1179.

Shin, D.H., and Dunston, P.S. (2009). “Evaluation of augmented reality in steel column inspection.” *Automation in Construction*, 18(2), 118-129.

Snavely, N., Seitz, S., and Szeliski, R. (2008). “Modeling the world from internet photo collections” *International Journal of Computer Vision*, 80(2), 189-210.

Tomasi, C., and Kanade, T. (2004). “Detection and tracking of point features.” *Pattern Recognition*.

Tsai, R.Y. (1987). “A versatile camera calibration technique for high-accuracy 3D machine vision metrology using off-the-shelf TV cameras and lenses.” *IEEE Transactions on Robotics and Automation*, RA-3(4), 323-344.

Viswanathan, M. (2005). *Measurement Error and Research Design*, Sage Publications, Thousand Oaks, CA.

Walton, J.S. (Ed.), (1990). “Image-based motion measurement.” *Proceedings of Symposium SPIE 1356*, University of California, San Diego, 144 pp.

Waugh, L. (2006). “Construction site photography: virtual reality vs. the focus+context problem.” *Proceeding of 2006 Annual CSCE Conference of the Canadian Society for Civil Engineering*, Page No: CT-092 1-8, Calgary, Canada.

Wolf, P. (1983). *Elements of Photogrammetry*, McGraw-Hill, New York.

Wong, K.W. (1980). “Basic mathematics of photogrammetry.” *Manual of Photogrammetry*, 4th ed., ed. C. C. Slama, ASPRS, Falls Church, VA, Chap. 2, 37-101.

Zhang, J.P., Anson, M., and Wang, Q. (2000). “A new 4D management approach to construction planning and site space utilization.” *Proceedings of the Eighth International Conference on Computing in Civil and Building Engineering*, California, USA, 15-22.

Zhu, Z., and Brilakis, I. (2009) "Comparison of civil infrastructure optical-based spatial data acquisition techniques", *Journal of Computing in Civil Engineering*, ASCE, 23(3), 170-177.